Draft version February 8, 2022
Typeset using LaTeX default style in AASTeX63

The Solar Neighborhood XLIX: New Discoveries and Orbits of M Dwarf Multiples with Speckle Interferometry at SOAR

Eliot Halley Vrijmoet,[1,2,*] Andrei Tokovinin,[3] Todd J. Henry,[2,*] Jennifer G. Winters,[4,*] Elliott Horch,[5] and Wei-Chun Jao[1,*]

[1] *Department of Physics and Astronomy, Georgia State University, Atlanta, GA 30303, USA*
[2] *RECONS Institute, Chambersburg, PA 17201, USA*
[3] *Cerro Tololo Inter-American Observatory — NSF's NOIRLab, Casilla 603, La Serena, Chile*
[4] *Center for Astrophysics — Harvard & Smithsonian, 60 Garden Street, Cambridge, MA 02138, USA*
[5] *Department of Physics, Southern Connecticut State University, 501 Crescent Street, New Haven, CT 06515, USA*

(Received ???; Revised ???; Accepted ???)

ABSTRACT

We present the first results of a multi-year program to map the orbits of M dwarf multiples within 25 parsecs. The observations were conducted primarily during 2019–2020 using speckle interferometry at the Southern Astrophysical Research (SOAR) Telescope in Chile, using the High-Resolution Camera mounted on the adaptive optics module (HRCam+SAM). The sample of nearby M dwarfs is drawn from three sources: multiples from the RECONS long-term astrometric monitoring program at the SMARTS 0.9 m, known multiples for which these new observations will enable or improve orbit fits, and candidate multiples flagged by their astrometric fits in *Gaia* Data Release 2 (DR2). We surveyed 333 of our 338 M dwarfs via 830 speckle observations, detecting companions for 63% of the stars. Most notably, this includes new companions for 76% in the subset selected from *Gaia* DR2. In all, we report the first direct detections of 97 new stellar companions to the observed M dwarfs. Here we present the properties of those detections, the limits of each non-detection, and five orbits with periods 0.67–29 yr already observed as part of this program. Companions detected have projected separations of 0.″024–2.″0 (0.25–66 AU) from their primaries and have $\Delta I \lesssim 5.0$ mag. This multi-year campaign will ultimately map complete orbits for nearby M dwarfs with periods up to 3 yr, and provide key epochs to stretch orbital determinations for binaries to 30 yr.

Keywords: Astrometric binary stars (79), Astrometry (80), Binary stars (154), M stars (985), Speckle interferometry (1552), Low mass stars (2050)

1. INTRODUCTION

Stars in binary and multiple star systems have been observed in many varieties of orbits, each the result of the stellar formation and dynamical evolution processes that guided them through to the present day. Multiples may form from fragmentation at overdensities in the collapsing molecular cloud (Pringle 1989), creating gravitationally bound stars separated by thousands of AU (Offner et al. 2016; Lee et al. 2019; Kuffmeier et al. 2019), or may form later from the fragmentation of the disk around a (single) protostar, generating stars separated by 50–200 AU (Bonnell & Bate 1994; Kratter et al. 2010). Observers, however, have noted a wealth of systems with separations of $\lesssim$10 AU, indicating that many of these multiples undergo significant dissipative processes to lose their angular momentum (Duchêne & Kraus 2013). As reviewed in Bate (2015) and Lee et al. (2020), such processes could involve close encounters with nearby stellar neighbors or interactions with the circumstellar or circumbinary disk(s), such as accretion, which in turn is affected by magnetic field interactions and metallicity (Moe et al. 2019).

Corresponding author: Eliot Halley Vrijmoet
vrijmoet@astro.gsu.edu

* Visiting Astronomer, Cerro Tololo Inter-American Observatory. CTIO is operated by AURA, Inc., under contract to the National Science Foundation.

Clarifying the roles of these processes requires detailed numerical models and, above all, observed distributions of the orbital parameters such as orbital period, semimajor axis, eccentricity, and mass ratio, that are affected by these dissipative processes. For example, a distribution favoring high eccentricities suggests a thermal distribution of orbital velocities produced by dominating dynamical interactions (Kroupa 2008), and has been observed for systems with early-type primary stars (Moe & Di Stefano 2017). Or, as a broader example, if the presence of a disk generally dampens eccentricity, then any trends of eccentricity with semimajor axis could be linked to disk size scales. Key information will come especially from the inclusion of higher-order multiples such as triples and quadruples, rather than binaries alone, as those systems carry additional evidence through their ratios of masses and orbital periods and the mutual inclinations of their orbits.

Previous efforts establishing orbital element distributions for main sequence multiples have focused on specific spectral type or mass regimes. For example, binaries of solar-type stars of types FGK were the focus of Duquennoy & Mayor (1991) and a succeeding effort by Raghavan et al. (2010). Results for early-type binaries with O primary stars were presented by Mason et al. (1998), with additional analysis that compared the O and B massive stars to the solar-type stars by Moe & Di Stefano (2017). Each of these efforts has discussed the observed distribution of eccentricity as a function of orbital period ($P_{\rm orb}$ vs. e), highlighting that solar-type and more massive systems show a clear correlation between period and eccentricity, with the shortest-period systems almost exclusively circular. In contrast, the very low-mass systems ($\lesssim$0.1 $M_\odot$) presented by Dupuy & Liu (2017) did not show this correlation. This result suggests a mass-dependent or age-dependent difference in dynamical histories or formation pathways of stellar multiples.

M dwarfs make up ∼75% of all stars (Henry et al. 2006, 2018), and a detailed study of their orbital architectures would complete the sweep of stars along the main sequence. With masses spanning 0.08–0.62 $M_\odot$ (Benedict et al. 2016), they are the primary product of the star formation process, so their ubiquity renders their orbital parameter distributions of particular interest. In an initial effort, M dwarf systems showed a solar-type $P_{\rm orb}$ vs. e distribution in Udry et al. (2000), but their results were limited by their small sample of 48 systems, and an expanded sample is needed.

To bolster the statistics for M dwarf multiples, we are assembling a sample of at least 120 M dwarf systems with accurately measured orbits spanning periods 0–30 yr and semimajor axes up to ∼10 AU (depending on stellar mass). This sample size makes this study the largest on M dwarf multiples' orbits to date. With a particular focus on orbital eccentricity, our goals include determining the period at which tidal circularization occurs and to reveal any structures in the $P_{\rm orb}$ vs. e diagram. Our specific goal is to determine 120 orbits in an attempt to populate the final $P_{\rm orb}$ vs. e plot with roughly 20 orbits in each 5-year bin of $P_{\rm orb}$, making the eccentricity distributions clear overall as well as within each of those regimes. The specific goal of 120 orbits has been set to maximize the detail of the final distribution with consideration for availability of resources. We are collecting these orbits from broader sets of multiples observed in the long-term RECONS (REsearch Consortium On Nearby Stars, www.recons.org) astrometry program (as described in Vrijmoet et al. 2020), known orbits in the literature (including the ∼30 published from the Udry et al. (2000) sample described above, and a new multi-epoch speckle interferometry campaign.

This paper presents the first results of the speckle observations, which are being carried out at the Southern Astrophysical Research (SOAR) 4.3 m telescope in Chile using the High-Resolution Camera (HRCam) and SOAR Adaptive Optics Module (SAM; Tokovinin 2018b). This productive telescope-instrument combination has been used to derive hundreds of high-quality orbits over the past decade (e.g., Tokovinin et al. 2019a, 2020b). Observations for this M dwarf project have progressed at a rapid pace since commencing in 2019, with orbital motion clearly visible already for several targets. The resulting characterization of M dwarf multiples, in parallel with our complementary multiplicity study of K dwarfs (Henry et al. 2021), will provide key comparisons between the lowest mass stars and their higher-mass cousins, as well as a data set well-suited to constraining formation and dynamical evolution models of multi-star systems. In this paper, we focus on the M dwarfs, describing the sample in §2, the speckle observations in §3, and results of the SOAR effort in §4. Discussion of the results proceeds in §5.

2. SAMPLE

The targets in this program are 338 known and candidate M dwarf multiples within 25 pc visible from the Southern Hemisphere. By the end of 2020, 333 of these targets have been observed at SOAR.

Distances were determined via parallaxes from the RECONS astrometry program at the SMARTS 0.9 m (§2.1 in this paper; also Jao et al. 2005; Henry et al. 2018) and *Gaia* DR2 (Gaia Collaboration et al. 2016, 2018); all systems

meet the 25 pc cutoff in one or both of these catalogs[1]. The full sample will be volume-limited, but does not need to be volume-complete. M dwarfs have been selected as having $V - K_s > 3.70$ using Johnson V and 2MASS K_s (hereafter K) filters, as well as absolute magnitude $M_V > 9.02$. These limits were established as the M_V and M_K values corresponding to 0.6 $M_\odot$ using the Benedict et al. (2016) mass-luminosity relation for M dwarfs. This sample thus spans spectral types M0 through M9. For 11 systems that had no V measurements available, we converted the *Gaia* DR2 B_G and R_G magnitudes to V using the relations for M dwarfs in Jao et al. (2018). Finally, the specifications of HRCam+SAM on SOAR limit the sample to systems brighter than $I = 14$ mag and south of $+25°$ in declination.

The primary goal of the project is to map the distribution of orbital eccentricity with respect to orbital period, with the sample of 338 systems intended to support an even representation of periods 0–30 yr. Although determining 120 accurate orbits is the primary goal, the speckle sample includes several times that many systems; this reflects our expectation that only a subset will have well-defined orbits with $P_{\rm orb} < 30$ yr by the end of the 3-year observing campaign. To reach 120 orbits, the full project sample will include orbits observed using additional methods from other programs with a variety of time baselines and strengths, e.g., long-term astrometry and systems with spectroscopic orbits. Because this paper presents results of the speckle subset only, hereafter the "sample" and similar terms will refer to the speckle subsample rather than the ultimate full project sample that will include all observing methods.

Table 1 lists the entire speckle sample of 338 M dwarfs targeted at SOAR, including the five stars not yet observed by the end of 2020. For each target are listed Right Ascension and Declination 2000.0 positions (columns 1–2), the WDS-style coordinate name (column 3), the WDS discoverer code if the pair has been previously resolved (column 4), and the target name used in other RECONS work (column 5). These identifying parameters are followed by each system's parallax in milliarcseconds (mas; column 6) and the reference for that value (column 7), the V magnitude and reference (columns 8 and 9), and the $V - K$ color (column 10), where K is from 2MASS (Cutri et al. 2003). Given next are the subsets to which each target belongs (columns 11–13, described in detail below) and flags (column 14) for whether the system has been resolved (Y) or not resolved (N) thus far at SOAR (N/A indicates not yet observed), with the flag "T2" marking systems with results presented in Table 2. Finally, a reference for the orbit of a system is given (column 15), if it exists, with flag "T4" in this column marking systems with orbits presented in this work (§4.3).

The target list of 338 systems is drawn from three sources: astrometric multiples identified through long-term RECONS data (Jao et al. 2005; Henry et al. 2018), known multiples from the literature with potential $P_{\rm orb} < 30$ yr, and suspected multiples chosen based on their *Gaia* DR2 results (criteria described in Vrijmoet et al. 2020). As illustrated in Figure 1, these subsets overlap each other — for example, some systems from RECONS astrometry are already known multiples in the literature — and in the target list in Table 1 we have indicated each target's subset membership using columns 11–13. The selection and goals for each of these groups is described next.

2.1. *123 Targets from the RECONS Astrometry Program*

The RECONS program (Jao et al. 2005; Henry et al. 2018) began taking astrometry data in 1999, targeting red, brown, and white dwarfs within 25 pc. Through 4–6 observing runs per year at the SMARTS 0.9 m at CTIO, this program has been mapping the motions of several hundred nearby stars for a median duration of 10 yr. This enables the detection of binaries with orbital periods many decades in length, with orbital characterization possible for $P_{\rm orb}$ up to ∼30 yr in the longest-observed cases. Fully observed orbits are fit using the Markov Chain Monte Carlo method introduced in Dieterich et al. (2018), which simultaneously fits the proper motion, parallax, and orbital motion of the system's photocenter; nine examples with $P_{\rm orb}$ from 2–17 yr using RECONS data from the 0.9 m are given in Vrijmoet et al. (2020).

RECONS astrometry qualified the selection of 123 targets for the SOAR observing list, with 37 of these targets not qualifying for either of the other two subsets. Systems were considered high priority if their residuals to the parallax and proper motion fit exhibited perturbations (PBs) that were characteristic of orbital motion due to bound companions. These residuals are considered significant perturbations if their maximum amplitude is at least three times the size of the average error per epoch for that system (with these errors typically 3–5 mas). In many cases these residuals clearly traced out orbital motion by the system's photocenter, with a smooth rise and fall in R.A. and/or Decl. axes, depending on orbital coverage, observing cadence, and the particular orbit shape. Orbital period can be estimated by eye in these cases, or constrained by a preliminary fit to an astrometric orbit model. Targets were

[1] A few systems do not meet the 25 pc distance cutoff using updated parallaxes from *Gaia* EDR3 (Gaia Collaboration et al. 2020), which was released after this SOAR program began.

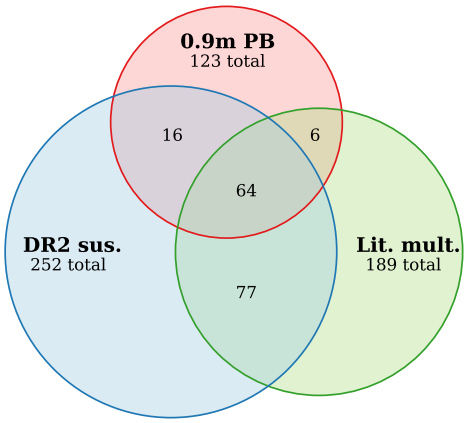

Figure 1. Venn diagram illustrating the three subsets of the SOAR sample of nearby M dwarfs. The area of each circle is proportional to the number of targets in that subset, but the overlapping regions are not to scale. Each circle is labeled with a reference to the subset's source: "0.9 m PB" for targets showing perturbations (PBs) in the RECONS astrometry program at the CTIO 0.9 m, "Lit. mult." for known literature multiples, and "DR2 sus." for systems suspected to be multiples based on their *Gaia* DR2 results. The number of targets is given under each subset name, and the numbers in the overlapping sections indicate the number of targets common to multiple subsets.

selected for our SOAR speckle campaign if these residuals thus indicated an orbit with likely $P_{\rm orb} \lesssim 30$ yr. In other select cases the residuals were clearly perturbed but the motion was more difficult to interpret, which may occur when an orbit shorter than ∼3 yr is observed with the relatively sparse cadence of the RECONS observations or the PB is weak because two components have similar fluxes and the photocenter consequently moves very little.

The goals for the "0.9 m PB" subset (column 11 in Table 1) are thus twofold:

- For systems with orbits that can be fully characterized in the RECONS astrometry, resolving the components will allow us to determine their individual dynamical masses (following the methods outlined in van de Kamp 1967).
- For targets with PBs that are ambiguous rather than clearly due to orbital motion, resolving a second star will confirm that companion and constrain its orbit, aiding interpretation of the RECONS astrometric residuals and ongoing observing priorities for the 0.9 m program.

In both cases, non-detections will place constraints on the natures of the potential companions and their orbits, and in some cases (notably, in the unclear ones) non-detections will allow us to rule out a companion as the source of the astrometric residuals.

2.2. *189 Targets from Known Multiples in the Literature*

To enrich the sample, and because astrometry is less sensitive to some types of binaries (e.g., equal luminosity components), the SOAR target list was augmented with known M dwarf multiples from the literature. These known multiples constitute 189 targets, with 42 not belonging to either of the other subsets. Our observations are intended to capture orbital motion, so these targets were limited to pairs that had previously been resolved at separations $\lesssim 2\farcs0$ or likely orbital periods less than 30 yr. Not all of these pairs have been resolved in the literature; about a third are known multiples based on only spectroscopic or astrometric results. These systems were primarily selected by cross-matching the Sixth Catalog of Orbits of Visual Binary Stars (Hartkopf et al. 2001) against coordinates of M dwarfs from *Gaia* DR2 and the RECONS astrometry target list. These were augmented by some M dwarf multiples from the Washington Double Star Catalog (WDS; Mason et al. 2001) and private communications from collaborators.

The intention of the observations for this "Literature multiples" subset (column 12 of Table 1) is to add new measurements to the existing data sets for each system, with the following goals:

- Enable fitting of each system's relative orbit by extending the time baseline of observations.
- Improve upon any existing orbit fits, in particular by refining the precision of the orbital elements.

2.3. *252 Targets Selected from Gaia DR2*

Gaia DR2 (Gaia Collaboration et al. 2016, 2018) released proper motions and parallaxes for ∼1.7 billion sources based on an astrometric model that includes only those two sources of motion, with orbital motion fits not planned until future data releases. Systems exhibiting orbital motion from a bound companion should thus exhibit evidence of poor astrometric fits. Vrijmoet et al. (2020) showed that nearby M dwarfs with unresolved companions can be selected based on several DR2 fit parameters, akin to the astrometric residuals in RECONS data (§2.1).

Gaia DR2 results were used to identify 252 total M dwarfs for the SOAR observing list, with DR2 being the only source of potential multiplicity for 95 targets. This evidence is based on the analysis of Vrijmoet et al. (2020), and most of these "DR2 suspects" met at least some of the final criteria presented there. Those specific DR2 criteria identified in Vrijmoet et al. (2020) were:

1. missing parallax or missing catalog entry,
2. `parallax_err` ≥ 0.32 mas for $G \lesssim 18$ (≥ 0.40 mas otherwise),
3. `astrometric_gof_al` ≥ 56.0,
4. `astrometric_excess_noise` ≥ 108.0, and
5. `ruwe` ≥ 2.0.

That work found that at least three out of four systems meeting at least one of these thresholds were multiples unresolved in DR2. While selecting targets for this subset of SOAR observations, we anticipated that the values of these criteria may eventually be lowered if many stars that were presumed single are later revealed to be binary.

The goals for this group of "DR2 suspects"(column 13 of Table 1) are:

- Map orbits of new multiples with periods that will be at least 50% complete by the end of this 3-year observing campaign (i.e., with $P_{\rm orb} \lesssim 6$ yr). The DR2 selection criteria should be more sensitive to these particular systems because of its relatively short observing baseline of 22 months.
- Confirm the validity of the Vrijmoet et al. (2020) criteria for selecting binaries from *Gaia* DR2 via the resolution of companions, and revise the criteria if necessary.

3. OBSERVATIONS AND DATA REDUCTION WITH HRCAM+SAM

The observations presented here were made over 2018–2020, with most completed between July 2019 and December 2020, representing the first half of our planned 3-year program. Many systems in our sample were already observed at SOAR prior to this project as part of earlier initiatives to investigate M dwarfs in the Southern Hemisphere. Their results do not appear in Table 2 because those results were presented in previous SOAR papers (Tokovinin et al. 2021, 2020b); instead, they have a "Y" or "N" in column 13 of Table 1 with no additional flags.

Time awarded for the speckle observing programs of coauthors Tokovinin and Vrijmoet was combined in order to increase the opportunities for timely observations of fast-orbiting systems. In preparation for each observing run, previous SOAR observations and RECONS astrometry were considered, and systems that had exhibited rapid orbital motion were prioritized for the upcoming run. This procedure improved the likelihood that defining features of the orbit shapes would not be missed.

All of the observations used HRCam, the high-resolution camera mounted on the SOAR Adaptive Module (SAM, Tokovinin et al. 2016b), in the seeing-limited mode (no laser guide star was used). Frames were taken almost exclusively in the Kron-Cousins I filter, usually in 2–3 sets (data cubes) of 400 frames per target, with integrations typically 24 ms per frame. These sets were each later processed independently to verify results. Most observations use the HRCam narrow 3″ field of 200×200 pixels, whereas pairs known to have separations of 1.″4 or more were observed with the 400×400 field. The resolution limit in I is usually 40–45 mas depending on target brightness and sky conditions, but can be as close as 35 mas in some cases (see Figure 1 of Tokovinin et al. 2020b). Targets that are unresolved in the first two attempts are usually observed a third time, then retired from the program if still unresolved.

The data are processed and reduced for this program using the standard procedures described in Tokovinin et al. (2010) and Tokovinin (2018b), and representative images of the reduced data products are shown in Tokovinin (2018b). In brief, for each target the power spectrum and autocorrelation function are calculated, and companions are noted via power spectrum fringes or secondary peaks in the autocorrelation function. Fitting an empirical model to the power spectrum yields the parameters of each detected pair: the separation between components (ρ), the position angle of the secondary with respect to primary star (θ) (north = 0° through east = 90°), and the difference in magnitude between components (Δm). Important details about these results are:

- The position angle determined through this procedure is only ascertainable modulo 180°, leaving some ambiguity in the secondary's true position on the sky. This ambiguity has been eliminated whenever possible by applying a shift-and-add procedure to each target's data (Tokovinin 2018b); this process reveals the true quadrant for companions that are not too faint but still have some magnitude difference with their primary star ($\Delta m \gtrsim 0$ mag). These results are noted with the "q" flag in Table 2, indicating that the quadrant has been determined.
- For some observations of wider pairs a separate procedure is used to determine the magnitude difference using the average image for a target (described in detail in Tokovinin et al. 2010). This method produces more reliable photometry for these cases where the stars' separations are greater than image resolution, reducing bias from speckle anisoplanatism. Observations with Δm determined with this method are marked by a "p" in Table 2, indicating that this photometric method has been used.
- For observations in which no companion was detected, a contrast curve is computed to report the detection (magnitude) limits as a function of the distance from primary star on the sky (for example, see Figure 5 of Tokovinin 2018b). The parameters of this curve are reported in the results in Table 2 as the minimum separation resolvable for pairs with $\Delta m < 1$ mag, as determined from the maximum spatial frequency of the power spectrum, and the maximum detectable magnitude difference at separations of 0.″15 and 1.″0 (the dynamic range).

4. RESULTS

Through the end of 2020 and including previously published results, 333 targets on this program have been observed at least once at SOAR via 830 total observations. Of these targets, 211 (63% of the total sample) had a companion detected at least once, representing 204 total systems[2]. In this first half of our 3-year program, most companions were observed numerous times to confirm that the detected object was a true companion and not a background source; the remainder have follow-up observations planned. For each true multiple, these initial observations will then contribute to that system's orbit mapping.

The results are detailed in Table 2 for both newly resolved and unresolved systems. Targets with previous resolutions appear instead in the yearly SOAR publication series (e.g., Tokovinin et al. 2020b, 2021). Table 2 gives the WDS coordinate name or anticipated WDS name in column 1. In column 2 is either the reference for the first resolution of that system, a single asterisk (*) for the first resolution of a known multiple, two asterisks (**) for the first resolution of a system that was previously, at best, only a candidate multiple (see §4.1 for details), or "none" if the system was not resolved. Each observation of a target is then distinguished by its date (column 3) and Y/N flag for whether or not the companion was detected at that epoch (column 4). Observations in which the companion was resolved include the separation, position angle, and magnitude difference between components (columns 5–7). Observations with no detected companion list the minimum resolution detectable and Δm limits at 0.″15 and 1.″0 from the primary star, respectively (columns 8–10). Finally, observation flags (column 11) note several of the cases described in §3, such as when the quadrant of the position angle is unambiguously determined (q), when the magnitude difference was determined photometrically from the average image (p), when the observations resulted in noisy data (:), generally leading to less robust limits, or y for the one observation done through a y filter rather than the I filter.

Uncertainties on the individual measurements are not listed here, as these would require a more detailed analysis than feasible for this paper. The full measurement errors consist of internal errors, which could be determined by comparing each observation's data cubes, and external errors, which can be estimated from HRCam measurements of well-characterized binaries ("calibrators"), *Gaia* resolved sources (Tokovinin et al. 2019a), and residuals of each system's orbital fit. The typical deviation of the calibrators from their orbit models is 1–3 mas in separation and 0.2°

[2] In seven cases, a higher-order multiple with two components separated by a few arcseconds represents two targets for this speckle survey, and as such is represented by two lines in Table 1 (and counts as two targets throughout this paper).

in position angle, and in a similar procedure with SOAR speckle data, Mann et al. (2019) found errors of 3.8 mas and 0.94° are appropriate additions to the internal errors (typically ≤2 mas). For this reason we have assigned errors of 5 mas to all SOAR HRCam measurements when fitting orbits, and postponed the full derivation of external errors until this 3-year observing program is complete. See §4.3 for additional details of the orbit fitting routine.

4.1. *Detections*

Table 3 summarizes the detection rates for each group within the full sample (§2). For each named subset (column 1), it provides the number of targets observed (column 2), the number resolved (column 3), the percentage of observed targets that were resolved (column 4), and the number of targets not yet observed by the end of 2020 (column 5).

Of the 211 companions resolved in our sample, 97 had no previously published resolutions, making these results their first published positional measurements. These newly resolved systems are marked with asterisks in column 2 of Table 2, broken into two categories. A single asterisk (*) denotes the 34 systems that were already reported to be multiples based on other published data, e.g., astrometry or spectroscopy. A double asterisk (**) denotes new resolutions for 63 systems with no previously reported multiplicity in the literature — these were included in the target list due to anomalies in their RECONS or *Gaia* DR2 astrometry. These are newly discovered multiples in addition to being new resolutions.

Additionally, 114 companions noted here as resolved at SOAR already had resolutions in the literature; nearly all of these systems are listed as "Y" in Table 1 but without the "T2" flag, as they are presented in Tokovinin et al. (2020b), Tokovinin et al. (2021), and previous publications in that yearly series. Column 2 of Table 2 gives the reference for the first resolution of that system. For all systems with data already in the literature, the new observations presented here and in the other SOAR results papers will ultimately be combined with previous results to improve orbital coverage. We have already employed this strategy for the orbits we are presenting here (§4.3).

Data from the RECONS astrometry program at the SMARTS 0.9 m already reveals perturbations in 59 of the 211 resolved pairs. That astrometry provides maps of the photocentric orbits, hence the resolutions of companions in these cases will enable us to solve for the individual masses within each pair as in, e.g., Dieterich et al. (2018). Each of these new masses will contribute to the currently modest number of dynamically determined individual M dwarf masses known to date (Benedict et al. 2016).

Finally, there are 249 targets observed (and 3 targets not observed) that showed some evidence of poor astrometric fits in *Gaia* DR2 and were included based on preliminary results of the Vrijmoet et al. (2020) analysis. Our SOAR observations reveal that 188 (76%) of these M dwarfs host a companion. This result highlights the utility of that method of selecting likely multiples using *Gaia*'s astrometric fit parameters, especially for these nearby, low mass systems. See §5.4 for further discussion of this result, details about the DR2 criteria outlined in Table 2, and the implications.

Figure 2 shows the separations (ρ) and magnitude differences in I band (ΔI) for each observation that detected a companion. This distribution of exclusively M dwarfs is similar to that of the wider sample observed yearly by SOAR (shown in Figure 1 of Tokovinin et al. 2020b). The most notable difference is our distribution shows a paucity of systems with $\Delta I > 1.5$ mag and $\rho < 0\farcs1$. This discrepancy could reflect the higher fraction of very faint companions in our sample compared to the other samples observed yearly at SOAR. The mass-luminosity relation is known to experience a severe drop at optical wavelengths at low M dwarf masses (Benedict et al. 2016). Therefore, it is not surprising that companions only slightly less massive than their primaries may have large ΔI values compared to their primaries and remain undetected at SOAR.

4.2. *Non-detections*

The 122 targets observed with no companions detected at SOAR still impart important information via the detection limits given in columns 8–10 of Table 2. Because these observations were conducted in the I filter, in many cases these non-detections restrict potential companions to the regimes of cool white dwarfs, very low-mass stars, or brown dwarfs. Examples include LHS 1582 AB (03434−0934), SCR 0723-8015 AB (07240−8015), and LP 848-50 AB (10427−2416), all of which exhibit clear orbital motion in their long-term astrometry (Winters et al. 2017; Vrijmoet et al. 2020). Other true multiples unresolved here may have orbits too tight to resolve, or have components positioned unluckily too close to each other on the sky at the epoch of observation. In each of these cases, the non-detection information given here provides constraints on orbits and companion masses that can be used in concert with other efforts to reveal information about any unseen and/or undetected companions.

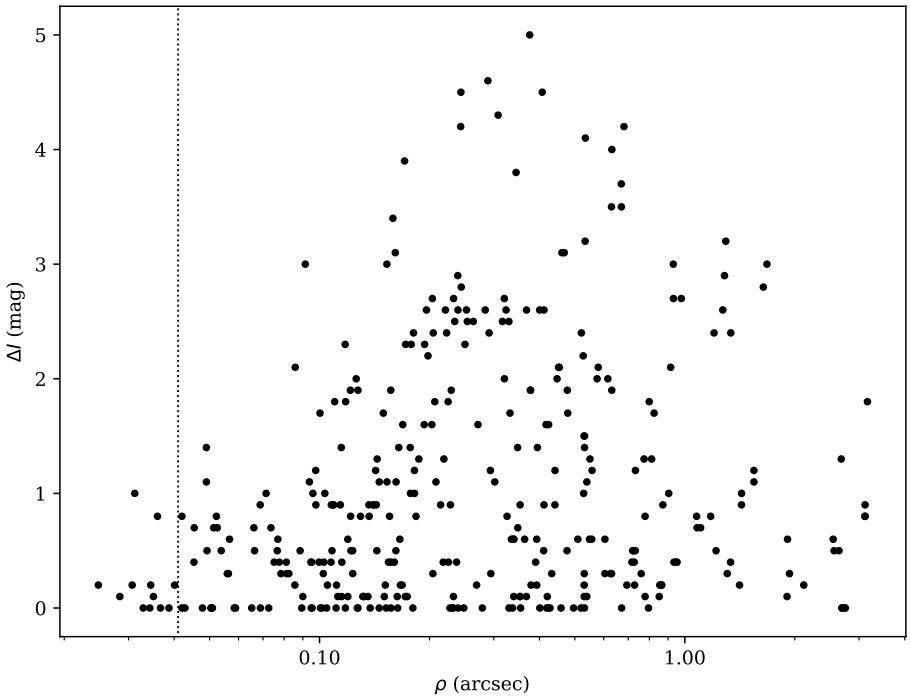

Figure 2. Separation ρ in arcsec and magnitude difference in I band for each observation that resolved a companion, excluding those for which the data were exceptionally noisy (":" flag in Table 2). The 41 mas formal diffraction limit of SOAR is indicated with the vertical dotted line. This sample is intentionally focused on the closer pairs ($\lesssim 1\farcs0$) that are more likely to show orbital motion over our 3-year campaign.

4.3. *Orbits*

Here we present five orbits fit using the SOAR observations, often combined with additional data available in the literature; all but LHS 501 AC are the first orbits for the systems. These five orbits represent the highest-quality fits possible with the data from this program thus far, and fortuitously are also representative of the range of size and time scales accessible to this program. The orbital periods range from 0.67–29 yr, and each has at least four observations taken during the first 1.5 years of this observing program. The full orbital parameters are given in Table 4 and illustrations of the fits are shown in Figure 3. Each dataset was fit with the `ORBIT` code (Tokovinin 2016a), which uses the Leavenberg-Marquardt least-squares method to identify the model orbit that best fits the weighted observations. The weights are inversely proportional to the errors on each point, which for these observations have been set to the typical external HRCam errors of 5 mas, and for literature observations are set to the published errors. The resulting fits have errors ranging from 0.3%–7.2% in orbital period and 1.3%–6.7% in semimajor axis. These errors on the orbital parameters are determined by the fitting algorithm.

Each system with an orbit fit is discussed briefly below. In each case we also provide estimates of the component masses using our work toward a mass-luminosity relation in I band (Vrijmoet et al. 2021). These estimates should be considered preliminary and are only intended as general guides of the mass regimes for these M dwarfs.

- G 131-26 AB (00089+2050, BEU 1) is a known flare star with a stellar companion first detected by Beuzit et al. (2004) in 2001, then resolved again in 2012 by Janson et al. (2014) and in 2014 by Horch et al. (2015). We have resolved it four additional times in 2019–2020 and fit all of these data together to determine an orbital period of 5.918 ± 0.017 yr. Combining this orbit with the *Gaia* EDR3 parallax indicates a total system mass of 0.51 ± 0.05 $M_\odot$. The individual components' M_I values are consistent with 0.3 $M_\odot$ and 0.2 $M_\odot$, a good match to the system total mass.

- 2MA 0015-1636 AB (00160−1637, BWL 2) was resolved by Bowler et al. (2015) in 2011, who suggested an orbital period of 4.5 yr based on their observed separation. With our additional five points we find an orbital period of 4.187 ± 0.039 yr, yielding a total mass of 0.41 ± 0.08 $M_\odot$ using the EDR3 parallax. The individual components'

absolute magnitudes imply masses of 0.25–0.3 $M_\odot$ for each component. These values are somewhat higher than indicated by the total dynamical mass, pointing to some inaccuracy in the orbit or the parallax. This is validated by the *Gaia* reduced unit weight error (RUWE) value of 4.1, indicating the parallax is not well fit. The mass discrepancy would be eliminated by a 7% smaller parallax, or by increasing the orbit's semimajor axis by 7% or decreasing its period by 10%. Continued observations at SOAR will allow us to refine the orbit, and future *Gaia* data releases will likewise improve the system's parallax.

- LP 993-115 BC (02452−4344, BRG 15Aa,Ab), also known as LP 993-116 AB, is a common proper motion companion to LP 993-115 A (44″; Bidelman 1985). The C component was first identified by Bergfors et al. (2010) with lucky imaging and resolutions also reported in Janson et al. (2012) and Janson et al. (2014). We add four new resolutions to map the other side of the orbit, and derive a period of 28.466 ± 2.056 yr. Using the EDR3 parallax, this suggests a total mass of 0.42 ± 0.23 $M_\odot$ for BC, although this value is poorly constrained. Individual absolute magnitudes for the B and C components are consistent with component masses of 0.2–0.25 $M_\odot$ each. This is the first orbit published for this subsystem of this higher-order multiple.

- SCR 0533-4257 AB (05335−4257, SYU 7Aa,Ab) was first resolved by Shan et al. (2017) in 2014, and to this we have added six points in 2019–2020. With an orbital period 0.672 ± 0.003 yr, the orbit and EDR3 parallax indicate a total mass of 0.40 ± 0.07 $M_\odot$. This is consistent with the possible period of 9 months noted in the unresolved RECONS astrometry by Riedel et al. (2018). The individual absolute magnitudes of each component are consistent with 0.25 $M_\odot$ and 0.15 $M_\odot$, together an excellent match to the total dynamical mass.

- LHS 501 AC (20556−1402) is a now-resolved primary with a wide companion known as LHS 500, separated by 107″ (Jao et al. 2003). The AC pair had not been resolved prior to this work, but was noted to be an astrometric multiple by Jao et al. (2011) based on the RECONS astrometry data. Baroch et al. (2018) noted it to be SB2 and presented a spectroscopic orbit fit. Our new orbit was fit to their spectroscopic data simultaneously with our four new visual resolutions using the same `ORBIT` code as for the other four orbits in this work. The resulting orbital period of 1.855 ± 0.014 yr is shorter in length but ten times more precise than the Baroch et al. (2018) period (2.22 ± 0.16 yr). Our eccentricity is also significantly different, at 0.242 ± 0.008 vs. their 0.402 ± 0.059. Additional observations underway will significantly improve future orbit fits for this system, as the radial velocity model still shows some minor discrepancies with the data (lower rightmost panel of Figure 3). With our result and the EDR3 parallax we derive a total mass of 0.37 ± 0.02 $M_\odot$. The individual absolute magnitudes correspond to stars with masses of 0.25 $M_\odot$ and 0.2 $M_\odot$, which is roughly consistent to the total dynamical mass, although future refinement will be necessary for this orbit.

5. DISCUSSION

As outlined in §1, our goal is to catalog at least 120 orbits with $P_{\rm orb} \leq 30$ yr with reliably determined orbital periods and eccentricities through the combination of this 3-year speckle campaign, the long-term RECONS astrometry program at the SMARTS 0.9 m, and orbits in the literature. A set representing orbits out to (at least) 30-year periods will be necessary to draw significant conclusions about the formation and evolution of these systems. Selecting 120 orbits evenly distributed in orbital period will ensure that there are ∼20 orbits in each 5-year bin of $P_{\rm orb}$ in the final $P_{\rm orb}$ vs. e plot. More fundamentally, the goal of 120 orbits is a compromise between the need to characterize the $P_{\rm orb}$ vs. e relation with maximum detail and a realistic expectation based on our prior experience and availability of resources.

The abundance of detected companions and promising initial orbit fits resulting from this first phase of our SOAR effort provide several advances toward the overall project regarding orbit distributions of M dwarf multiples. For all systems in Table 2, both the resolutions and non-resolutions reported here provide valuable constraints on the orbits of their companions or the likelihood of each star's multiplicity. Notably, we have increased the total number of resolved M dwarf multiples within 25 pc by 97, representing 194 targets for further study of M dwarf multiples' properties. We have also secured observations for 140 systems that had been previously resolved, providing not only new points for orbit determinations, but relative fluxes in the I band that can be used for a robust mass-luminosity relation at I. Finally, the five new orbits presented here can be added to the key $P_{\rm orb}$ vs. e plot, and each new fit helps to identify reliable orbits as well as those for which more data are required to reach the orbital element precision needed to reveal clues about the star formation process.

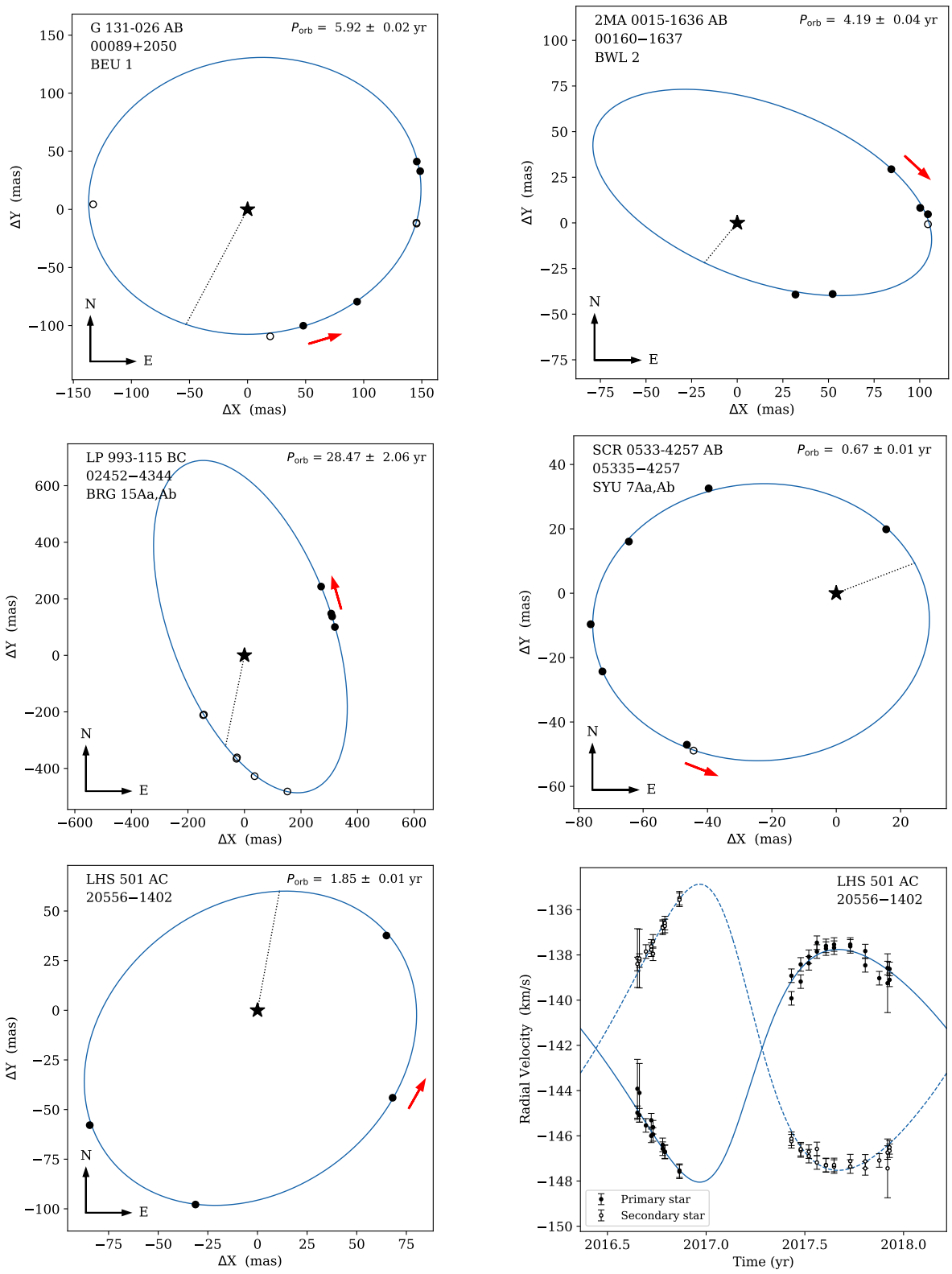

Figure 3. Five visual orbits for binaries resolved at SOAR, plus one spectroscopic orbit that was fit simultaneously with the corresponding visual orbit for LHS 501 AC. For the visual orbits, blue lines denote the fit, filled circles are SOAR observations, and open circles are observations added from the literature. Red arrows indicate the direction of motion of the secondary star around the primary, and the black star and dotted line denote the primary star and line of periastron. In the spectroscopic orbit (bottom right panel), the points and solid line are the observations and fit, respectively, for the primary component, and the open points and dashed line are the observations and fit for the secondary. *Left to right, top to bottom:* G 131-26 AB, 2MA 0015-1636 AB, LP 993-115 BC, SCR 0533-4257 AB, LHS 501 AC visual orbit, and LHS 501 AC radial velocity orbit (observations from Baroch et al. 2018). Sources for additional visual observations are specified in Table 4.

5.1. *Contributions to Nearby M Dwarf Orbits*

As of July 2021, ∼200 orbits in the Sixth Catalog of Orbits of Visual Binary Stars (Hartkopf et al. 2001) are those of M dwarf systems within 25 pc. About one third of these have periods longer than 100 yr, and another third have periods 10–100 yr, with the remaining third shorter than 10 yr. Our SOAR program targeting orbits 0–6 yr is thus well poised to make a significant contribution to this catalog. All but one of the orbits presented here have $P_{\rm orb}$ in that range, demonstrating proof of concept for this plan.

Four of the five orbits presented here are new, while the fifth (LHS 501 AC) represents a substantial revision over the previously published result (Baroch et al. 2018). This set of orbit results is roughly representative of the expected yield of our program: for most orbits, we will combine existing data with our new data to produce fits for systems that previously had no published orbits. Several dozen more orbits will be updates to systems that already had solutions published; these will be a substantial fraction of the 73 targets in our sample that already have orbits in the literature listed with $P_{\rm orb} \leq 30$ yr.

Overall, we expect to fit at least ∼50 orbits using the full three years of observations planned for this program. This estimate is based on the number of systems already showing substantial motion over the first 1.5 yr of observations and includes improvement of published orbits as well as new orbits. These will substantially contribute to the 120-orbit goal to establish the M dwarf $P_{\rm orb}$ vs. e distribution, supplementing the planned contributions from RECONS astrometry and the literature.

5.2. *Implications for the RECONS Astrometry Subset (0.9 m PB)*

Of the 120 systems observed from the 0.9 m PB list, 59 companions were detected using SOAR. Among these, 22 (37%) had not been resolved previously. The lower yield of this subsample compared to the other two is not too surprising because astrometry and speckle interferometry are each somewhat sensitive to different types of companions. Speckle searches are most sensitive to equal-luminosity components, but those systems exhibit no astrometric perturbation if both components are equal luminosity and have the same mass. In addition, many of the astrometric companions are likely very low mass stars or brown dwarfs that are beyond the magnitude difference limits of the speckle observations.

When no companion is detected with speckle, the magnitude limits reached at various separations constrain the nature of the astrometric companion and its orbit. Many cases in which these estimated mass limits were notable are described in detail in the Appendix (§A). For each system, we have used the combined magnitude of the pair and the limiting magnitudes in the speckle results to estimate the components' fluxes, which we then combine with the size of the astrometric perturbation to estimate a limit for each companion mass (following van de Kamp 1967). Most of these systems have been described in previous work in *The Solar Neighborhood* series, often with plots showing their perturbed astrometric residuals, hence our descriptions here can be considered updates to those notes.

We used a similar procedure to estimate companion masses for the 0.9 m PB systems that SOAR did resolve. These masses (given in §A) are only rough estimates determined from the sizes of the photocentric displacements in the astrometric pertubations, rather than the fully characterized photocentric orbits. Future work will determine reliable photocentric orbits that can be combined with these SOAR resolutions to yield dynamical masses for the individual components.

5.3. *Implications for the Known Literature Multiples Subset*

Of the literature multiples, 140 out of 188 pairs observed were resolved at SOAR. These resolutions were the first ever for 34 of these systems, while 106 had been previously resolved by others. Of the 48 unresolved systems, nearly all were initially identified as multiples through JHK imaging or spectroscopic studies, hence their companions were likely too faint (e.g., brown dwarfs) or too closely bound (spectroscopic binaries) to resolve at SOAR in I band. The new resolutions are systems that often have complementary (non-imaging) data in the literature, and the previously-resolved systems have imaging that precedes our SOAR results. Both cases will assist in our orbit fitting goals, as this extra information or lengthened time baseline both enable orbit fits to be made earlier than with our SOAR data alone. The five orbits presented here demonstrate that concept.

Our selected 30-year orbital period limit is meant to capture as broad a picture of M dwarf orbits as is feasible for a single observational program, in particular showcasing systems that fall between the widest binaries and those that are tightly bound because of tides. Inevitably, some of the systems we have resolved will prove to have orbits longer than our planned 30-year limit, as many of these are wider pairs initially detected with less sensitive instruments. In these

cases, the data from this campaign can be used to place constraints on those orbits, e.g., choosing appropriate cadences on these slow-moving systems to focus observations at future epochs when a companion moves quickly through its periastron passage. The ultimate contribution of multi-decade orbits will thus come through observations collected over multiple projects, with updated orbits more precisely determined than currently possible. For now, our SOAR observations of these literature multiples provide a legacy dataset that will contribute to future efforts long after our project is complete.

Long orbits can often be constrained by comparing their motions measured at two widely separated moments (e.g., Brandt et al. 2019; Currie et al. 2020; Bowler et al. 2021). These recent efforts use the *Hipparcos-Gaia* Catalog of Accelerations (HGCA; Brandt 2021), which has presented recalibrated proper motions of systems measured by the *Hipparcos* and *Gaia* missions, ∼30 years apart. Another catalog based on the same principle has been compiled by Kervella et al. (2019). There are 60 systems on our program with an entry in the HCGA and many of these likely have accelerations evident in that catalog. By combining positional measurements with these proper motion changes, we could better constrain the orbits of these systems, especially those with very long periods. We will consider the use of this approach in our future work on orbits.

5.4. *Checking Criteria for Unresolved Multiples in Gaia DR2*

A total of 249 of the 252 systems were observed from the DR2 suspects sample, selected at least partly based on their *Gaia* DR2 astrometric fits (91 stars were included based *only* on those fits). This subset was created because during the SOAR sample construction, the then-preliminary results of the Vrijmoet et al. (2020) analysis showed specific DR2 parameters to be reliable markers for unresolved multiplicity. The SOAR observations validate the defined markers, with companions detected for 188 stars (76% of that group). Many of these systems had no previously published resolved companions and are marked with ** in column 2 of Table 2.

The final analysis of Vrijmoet et al. (2020) ultimately listed five criteria that could be used to flag likely multiples in DR2 (given explicitly in §2.3): missing parallax or missing DR2 entry, and four threshold values of the DR2 astrometric fit parameters. That work involved constructing a sample of 542 RECONS parallax program targets that were cross-matched with *Gaia* DR2 results, and used those targets' multiplicity information to identify the DR2 astrometric fit parameters that best indicated the presence of unresolved companions. For each of these four identified parameters, threshold values were then determined, above which three out of four systems were unresolved multiples.

Of the 252 systems in our sample flagged in the preliminary stages of that DR2 analysis, 217 of the stars observed fulfill two or more of the final Vrijmoet et al. (2020) criteria. SOAR detected companions for 176 (81%) of these 217 targets, confirming that the majority of poor fits in DR2 were due to companions bright enough to detect with SOAR's HRCam+SAM. As *Gaia*'s observing time baseline increases with future data releases, these fit flags will reveal multiples with longer orbital periods and fainter companions (smaller masses), as long as the *Gaia* data are fit with the single-star astrometric model. Clearly, *Gaia* data can be used to reveal many new potential stellar multiples before the final release of its binary star solutions.

For the 41 of 217 observed systems that fulfilled at least two of the criteria from Vrijmoet et al. (2020) but did not have a companion resolved, the presence of a companion cannot be fully ruled out. Indeed, roughly half of this subset have had their companions already confirmed through other means, such as spectroscopically or by showing unambiguous orbital motion in RECONS astrometry. Companions that are very faint or orbiting close to their primary stars will not be detectable with HRCam+SAM at SOAR; the largest magnitude difference observed here was $\Delta I = 5.0$ and the smallest separation seen was 24 mas. The DR2 suspects marked unresolved in Table 1 must still be regarded as likely multiples, and future observations are warranted to probe for very faint and very close-in companions.

To update the criteria for unresolved multiplicity of *Gaia* DR2 targets, we have added the new SOAR detections to the sample used in Vrijmoet et al. (2020). Although the sample used in that analysis was not volume-complete beyond 13 pc, its proportion of multiples within any distance matched the observed multiplicity found by more comprehensive surveys (Winters et al. 2019). To preserve that feature and avoid overreporting multiples, we have updated the sample with these new detections by only updating the multiplicity information for the existing targets, without adding to that sample any new targets that may have been observed here. This sample multiplicity update does not substantially change the Vrijmoet et al. (2020) results. The threshold values of the four useful DR2 parameters may be lowered by ∼10% to select samples in which three out of four systems are unresolved multiples. The fifth criterion of missing DR2 entry or parallax remains valid. This consistency speaks to the robustness of the overall results of Vrijmoet et al. (2020).

6. CONCLUSIONS

In this work we have presented observations from the first 1.5 yr of our planned 3-year speckle interferometry campaign at SOAR to observe M dwarfs within 25 pc. Key results to date include:

- speckle measurements of 333 M dwarfs in 320 systems; 211 (63%) of these M dwarfs were resolved
- four new orbits and one revised orbit with periods of 0.67–29 yr for M dwarfs with masses of 0.15–0.30 $M_\odot$
- measurements of resolved companions for 76% of candidate multiples from *Gaia* DR2 identified by criteria for their astrometric fit parameters, as described in Vrijmoet et al. (2020)

Each observation reported here of a stellar companion is a step toward our goal of mapping the orbits of nearby M dwarf multiples. Our project specifically targets M dwarf systems with orbital periods of 0–30 yr and semimajor axes 0–6 AU and the five orbits presented here span this full range, including some of the fastest-orbiting in our sample and some with the richest sets of similar observations in the literature. Many systems had already been observed at SOAR prior to this project and have measurements described in recent papers (e.g., Tokovinin et al. 2020b, 2021). HRCam+SAM at SOAR has had many successful years observing stellar multiples (10 yr as of Tokovinin 2018b), and by focusing on the lowest-mass stars here we have thoroughly demonstrated its capabilities regarding faint, red systems.

Since the preparation of this paper began, with each observing run we have noted more systems that have enough data for orbit fits. This speckle program is thus well on its way to forming a significant contribution to the overall project of mapping M dwarf orbits, and we anticipate continued success in the remaining 1.5 yr of this program. A future publication at the conclusion of this campaign will include several times the number of orbits presented here.

This project is an effort bringing together several observing methods, and as such demonstrates the power of these methods to complement and inform each other. Long-term ground-based astrometry from RECONS provides many full orbits and highlights systems with anomalous motion (but not necessarily distinguishable orbits) for speckle follow-up. The speckle interferometry from SOAR confirms or constrains those systems, and also efficiently captures the equal-mass systems that are not easily detectable via unresolved astrometry. Speckle observations may be combined with other resolutions in the literature, e.g., from adaptive optics, allowing orbits to be observed and characterized over long time baselines.

A multi-method approach is essential to this project, as the spatial scales involved in binary star formation and dynamical evolution span orders of magnitude in AU. The complex mix of physics may depend on several fundamental properties such as mass, system mass ratio, and age, making it imperative that a wide range of orbits be considered to make meaningful comparison between models and observations. Ultimately, the multiples reported here have far-reaching potential consequences for M dwarf multiplicity, star formation, and local Galaxy mass distribution. This is because M dwarfs dominate the Galactic population, accounting for three out of every four stars (Henry et al. 2006, 2018). It is therefore essential to use all of the observing techniques at our disposal to determine not only which systems have companions, but to measure accurate sizes and shapes for their orbits, as those clues will reveal how the systems formed.

ACKNOWLEDGMENTS

Colleagues at the Southern Astrophysical Research (SOAR) Telescope, the Cerro Tololo Inter-American Observatory (CTIO), and the SMARTS Consortium and have made this work possible.

This work has made use of data from the European Space Agency (ESA) mission *Gaia* (https://www.cosmos.esa.int/gaia), processed by the *Gaia* Data Processing and Analysis Consortium (DPAC, https://www.cosmos.esa.int/web/gaia/dpac/consortium). Funding for the DPAC has been provided by national institutions, in particular the institutions participating in the *Gaia* Multilateral Agreement.

This research has made use of the Washington Double Star Catalog maintained at the U.S. Naval Observatory.

The National Science Foundation has been consistently supportive of this effort under grants AST-0507711, AST-0908402, AST-1109445, AST-141206, AST-1715551, and AST-2108373.

Facilities: CTIO:0.9 m, CTIO:SOAR

APPENDIX

A. SYSTEMS WORTHY OF NOTE

Here we describe several systems for which these SOAR results add significant new information or shed light on unusual observational histories. They are listed in order of ascending R.A., with WDS coordinate designations given in parentheses. The RECONS astrometry program mentioned for many systems refers to the long-term effort at the SMARTS 0.9 m.

- SCR 0128-1458 AB (01287−1458):

  Through four resolutions at SOAR, we have confirmed the presence of this companion first noted tentatively in RECONS astrometry residuals by Riedel et al. (2018). The ΔI of 2.6–2.7 mag indicates the companion has mass $\lesssim$0.2 $M_\odot$. Continuing observations will provide valuable future constraints for the photocentric orbit in the RECONS astrometry, which is still incomplete after 10 yr of data.

- LEHPM 1-1882 AB (01477−4836):

  Winters et al. (2017) revealed this binary via RECONS astrometry residuals. Its period is long, with the orbit not yet complete in what is now 15 yr of data. Although Winters et al. (2017) suggested the secondary companion contributes little light in R band, our three SOAR resolutions at I indicate a stellar companion with luminosity similar to the primary.

- LHS 1561 AB (03347−0451):

  Seven SOAR observations over 2018.8–2020.9 have resolved this system's secondary to have moved 20° through its orbit. Jeffers et al. (2018) reported this system to be a spectroscopic triple; the tertiary is presumably less luminous and/or more closely bound to the primary, as our observed component's motion and ΔI indicate that we are consistently resolving the same (secondary) companion.

- LHS 1582 AB (03434−0934):

  This system's 5 yr photocentric orbit was fully characterized in Vrijmoet et al. (2020), but the companion was not detected in our two SOAR observations. Comparison of the photometric (13 pc) and trigonometric (20 pc) distances by Riedel et al. (2010) and Lurie et al. (2014) indicated that the companion contributes noticeable light to the system. The limiting ΔI values of 1.4 mag at 0.″15 and 4.3 mag at 1.″0 from SOAR suggest it has mass $\lesssim$0.15 $M_\odot$.

- GJ 1068 (04105−5336):

  Two observations of this target revealed a relatively closely separated background star; at 2019.6136 its separation and position angle were 3.″7177 and 38.6°, and at 2020.1111 they were 5.″1628 and 35.5°. Comparison with archival images from the CTIO/SMARTS 0.9 m confirm that this background star is not bound to GJ 1068. This target's results are thus not included in Table 2.

- SCR 0702-6102 AB (07028−6103):

  We identified this system's companion early in the SOAR program as a fast mover, and have resolved it seven times from 2019.86–2020.99. The companion creates a low-amplitude perturbation in the RECONS astrometry residuals (as noted in Winters et al. 2017) with a period of ∼2.5 yr. That motion is consistent with what we have observed in the SOAR data.

- SCR 0723-8015 AB (07240−8015):

  This system's color and absolute magnitude are consistent with a ∼0.1 $M_\odot$ star, and the clear perturbation indicates an orbital period that has not yet wrapped in 17 years of RECONS astrometry data. The companion has not been detected in three observations in I at SOAR to limits of $\Delta I = 1.6$ and 3.0 at $0\farcs15$ and $1''$, respectively, indicating that it is of very low mass. This implies that the companion is a very low luminosity red or white dwarf, or a brown dwarf.

- SCR 0838-5855 AB (08380−5856):

  The RECONS astrometry indicates a large perturbation first shown in Winters et al. (2017) that now exceeds 50 mas in both RA and Decl. directions, but has not wrapped in 14 years of coverage. The two new SOAR resolutions are the first ever for this system and indicate the companion has $M_I = 14.6$, placing it very near end of the main sequence with a mass $\lesssim$0.1 $M_\odot$.

- LHS 2071 AB (08553−2352):

  This system was first noted as binary by Riedel et al. (2010), who presented a preliminary fit to the partially observed orbit in RECONS astrometry data. Ten additional years of data have revealed the orbital period to be greater than the 21 years of coverage to date. The four SOAR observations show clear orbital motion from 2018.2–2020.8; these will allow us to constrain the incomplete photocentric orbit in future work. The consistent ΔI of 2.4–2.6 mag indicate the companion has mass $\lesssim$0.2 $M_\odot$, but it is not substellar.

- LP 788-001 AB (09314−1718):

  Winters et al. (2017) showed clear orbital motion for this system in the RECONS astrometry residuals, and noted that the companion must contribute little flux in I band. The orbit has not wrapped after 8 years of coverage, and our SOAR observation in I did not reveal the companion. Because the absolute magnitude of this system sets the primary mass at ∼0.1 $M_\odot$, the detection limits suggest that the companion is substellar.

- LP 848-050 AB (10427−2416):

  This system exhibits an ∼8 yr orbit in the RECONS astrometry with a large-amplitude photocentric perturbation (see Figure 8 of Winters et al. 2017). Because the color and absolute magnitude of the system are consistent with a ∼0.1 $M_\odot$ star, the two non-resolutions at SOAR suggest that the companion is either a very low luminosity red or white dwarf, or a brown dwarf.

- L 327-121 AB (12336−4826):

  The RECONS astrometric perturbation for this system shown in Winters et al. (2017) has continued in recent data now spanning 10 yr. This is likely the reason this system has a poor fit in *Gaia* DR2 and no parallax given in EDR3. The orbital period is ∼9 yr, and a robust fit of this orbit will be possible in future work, enabling dynamical masses to be determined by combining that fit with these three new SOAR resolutions. Winters et al. (2017) noted an excessive mismatch between photometric and trigonometric distance, suggesting either that the system is young or includes a third luminous component. The SOAR data indicate M_I values of 8.43 and 8.83 for the two components, implying masses of 0.4–0.5 $M_\odot$ and 0.3–0.4 $M_\odot$. The mass sum is consistent with the orbital information available, indicating that a third luminous component is unlikely.

- LTT 6288 (15457−4330):

  This system's photocentric orbit was first described in Winters et al. (2017) and later updated in Vrijmoet et al. (2020). The orbital period is 9.9 yr. The two resolutions at SOAR indicate the companion's luminosity is consistent with mass $\lesssim$0.2 $M_\odot$, with the primary roughly twice as massive. The reliable RECONS astrometric

orbit and continuing SOAR observations will enable a precise dynamical mass determination for both components in future work.

- SCR 1546-5534 AB (15467−5535):

  The orbit shown in Henry et al. (2018) has continued in now 9 years of RECONS astrometry, with preliminary fits suggesting an orbital period of ∼7 yr. The two SOAR resolutions reveal the companion to be somewhat less massive than the primary star, with the secondary's absolute I magnitude consistent with $\lesssim$0.1 $M_\odot$ and the primary's consistent with roughly twice that mass. The secondary is more likely stellar than substellar, however, as Henry et al. (2018) pointed out overluminosity evident in the ∼30% difference between photometric (7 pc) and trigonometric (10 pc) distances for this system.

- LHS 3117 AB (15474−1054):

  Zechmeister et al. (2009) noted a radial velocity trend in VLT+UVES (Ultraviolet and Visible Spectrometer) data over ∼500 d starting in 2004, and noted this system as SB1. This signal was confirmed by the re-analysis of the same data by Tuomi et al. (2014). Our three new observations at SOAR over 2019.5–2020.2 reveal the companion, and the ΔI of 0.8–1.0 mag indicates it is likely a low-mass star rather than a brown dwarf.

- GJ 1212 AB (17137−0825):

  This system has been noted as a spectroscopic binary by Reiners et al. (2012), Houdebine & Mullan (2015), and Jeffers et al. (2018). No relative positions have been published before our SOAR observations. These three resolutions show component B moving quickly around A from 2019.5–2020.2, sweeping through 191° in position angle. Estimating the orbital semimajor axis to be 1–3 times the maximum displacement seen so far and assuming mass sums of 0.5–0.7 $M_\odot$ yields orbital periods of 0.97–5.9 yr. This target is thus high priority for continued observations and orbit characterization on our SOAR program.

- G 154-043 AB (18036−1859):

  Revealed as binary via the astrometric perturbation shown in (Winters et al. 2017), 10 years of RECONS data now show this system to have an orbital period of 8–12 yr. The two observations at SOAR indicate that this binary has components with M_I = 10.57 and 11.92, implying masses of 0.15 $M_\odot$ and 0.12 $M_\odot$. The SOAR data also show significant motion through 27°, so future work should allow for a refined orbit and reliable masses.

- LTT 7434 AB (18460−2856):

  As highlighted in Winters et al. (2017), this system has historically been challenging to interpret. The trigonometric distance is 1.4 times the photometric distance, implying two equal-mass components, yet the strong astrometric perturbation is only possible with unequal-mass components. Additional RECONS astrometry data acquired since Winters et al. (2017) continues the perturbation shown there, with the orbital period now estimated to be more than 20 yr. At SOAR we have twice resolved a companion at 0.″35–0.″39 (2019.61–2020.77) that is 1.4 mag fainter than the primary in I band; these are the first resolutions of this system. Bonfils et al. (2013) noted that this system is an SB2 with variable line width, suggesting the possibility of a close third component that could explain the excess flux. We will continue monitoring the long-term astrometry to complete the orbit and to look for any additional perturbations from a potential third companion.

- GJ 829 AB (21296+1739):

  Delfosse et al. (1999) first reported this system to be binary and characterized its spectroscopic orbit. It was reported as visually resolved by Oppenheimer et al. (2001) at Palomar and by Dieterich et al. (2012) with HST/NICMOS, but in both cases no details of the resolutions are given. Our SOAR observations of the companion at 25.0–36.7 mas separations are the most detailed to date. The close separation of this system presents a challenge for HRCam+SAM to resolve consistently, but its 53-day orbital period (Delfosse et al. 1999) give us ample future opportunities to attempt observations. When we have observed the entire orbit visually, fitting that data will yield the orbital inclination, which we will combine with the Delfosse et al. (1999) spectroscopic fit to obtain the individual component masses.

- LHS 3739 BC (21588−3226, a.k.a. LHS 3738 AB):

  The A-BC separation is 113″, forming a hierarchical triple. Riedel et al. (2010) first announced the companion to B based on RECONS astrometry and noted no significant overluminosity, indicating a much lower-mass companion. Lurie et al. (2014) presented an updated photocentric orbit; the six additional years of RECONS astrometry since then are consistent with that result. The BC pair has not been resolved at SOAR in two attempts, with limits of $\Delta I = 2.3$ at 0.″15 and 3.4 at 1.″0, implying a companion with mass lower than ∼0.1 $M_\odot$.

- LEHPM 1-4771 (22302−5345):

  Although this binary's orbital motion was shown in Winters et al. (2017) and its orbit fit updated in Vrijmoet et al. (2020), the five SOAR observations reported here represent the first resolutions of the pair. The magnitude difference of $\Delta I = 0.9$–1.2 mag indicates a secondary somewhat less massive than the primary, consistent with the assertion in Winters et al. (2017) that the secondary must contribute little flux in the R band. Once more of the ∼6 yr orbit is covered with SOAR observations, we will combine the photocentric fit with SOAR resolutions to determine dynamical masses for the components.

- LTT 9084 AB (22351−4218):

  This system was first resolved by Karmakar et al. (2020) in July 2013, who found the binary to be separated by 398–405 mas with position angle 333°–334°, and brightness differences of <0.2 mag in each of JHK bands. Our SOAR observations yield $\Delta I = 0.0$, consistent with the near-infrared values. Thus, the components are likely of similar mass. Our observations spanning 2019.5–2020.8 show the secondary moving from 428 mas to 401 mas, to nearly the same separation as observed in 2013 by Karmakar et al. (2020). The position angles we observed, however, were 17°–21° greater than the 2013 observations, increasing through 2019.5–2020.8. This displacement suggests the companion passed through due north in the 6 yr between 2013 and 2019. Together, the available data suggest the orbit is either highly inclined or highly eccentric. Although the orbit is likely several decades in duration, continued observations over the next two years could rule out one of the above scenarios through any variations in the secondary's speed.

REFERENCES

Andrade, M. 2007, RMxAA, 43, 237

Baroch, D., Morales, J. C., Ribas, I., et al. 2018, A&A, 619, A32. doi:10.1051/0004-6361/201833440

Bate, M. R. 2015, Living Together: Planets, Host Stars and Binaries, 496, 37

Benedict, G. F., Henry, T. J., Franz, O. G., et al. 2016, AJ, 152, 141

Bergfors, C., Brandner, W., Janson, M., et al. 2010, A&A, 520, A54. doi:10.1051/0004-6361/201014114

Beuzit, J.-L., Ségransan, D., Forveille, T., et al. 2004, A&A, 425, 997. doi:10.1051/0004-6361:20048006

Bidelman, W. P. 1985, ApJS, 59, 197. doi:10.1086/191069

Bonfils, X., Delfosse, X., Udry, S., et al. 2013, A&A, 549, A109. doi:10.1051/0004-6361/201014704

Bonnell, I. A. & Bate, M. R. 1994, MNRAS, 269, L45. doi:10.1093/mnras/269.1.L45

Bowler, B. P., Liu, M. C., Shkolnik, E. L., et al. 2015, ApJS, 216, 7. doi:10.1088/0067-0049/216/1/7

Bowler, B. P., Cochran, W. D., Endl, M., et al. 2021, AJ, 161, 106. doi:10.3847/1538-3881/abd243

Brandt, T. D., Dupuy, T. J., & Bowler, B. P. 2019, AJ, 158, 140. doi:10.3847/1538-3881/ab04a8

Brandt, T. D. 2021, ApJS, 254, 42. doi:10.3847/1538-4365/abf93c

Burgasser, A. J., Melis, C., Todd, J., et al. 2015, AJ, 150, 180. doi:10.1088/0004-6256/150/6/180

Calissendorff, P., Janson, M., Köhler, R., et al. 2017, A&A, 604, A82. doi:10.1051/0004-6361/201730725

Cutri, R. M., Skrutskie, M. F., van Dyk, S., et al. 2003, VizieR Online Data Catalog, II/246

Currie, T., Brandt, T. D., Kuzuhara, M., et al. 2020, ApJL, 904, L25. doi:10.3847/2041-8213/abc631

Dahn, C. C., Harrington, R. S., Kallarakal, V. V., et al. 1988, AJ, 95, 237. doi:10.1086/114633

Delfosse, X., Forveille, T., Beuzit, J.-L., et al. 1999, A&A, 344, 897

Dieterich, S. B., Henry, T. J., Golimowski, D. A., et al. 2012, AJ, 144, 64. doi:10.1088/0004-6256/144/2/64

Dieterich, S. B., Weinberger, A. J., Boss, A. P., et al. 2018, ApJ, 865, 28

Dittmann, J. A., Irwin, J. M., Charbonneau, D., et al. 2014, ApJ, 784, 156. doi:10.1088/0004-637X/784/2/156
Docobo, J. A., Gomez, J., Campo, P. P., et al. 2019, MNRAS, 482, 4096. doi:10.1093/mnras/sty2704
Duchêne, G., & Kraus, A. 2013, ARA&A, 51, 269
Dupuy, T. J., Liu, M. C., Bowler, B. P., et al. 2010, ApJ, 721, 1725. doi:10.1088/0004-637X/721/2/1725
Dupuy, T. J., Forbrich, J., Rizzuto, A., et al. 2016, ApJ, 827, 23. doi:10.3847/0004-637X/827/1/23
Dupuy, T. J. & Liu, M. C. 2017, ApJS, 231, 15. doi:10.3847/1538-4365/aa5e4c
Duquennoy, A. & Mayor, M. 1991, A&A, 500, 337
Forveille, T., Beuzit, J.-L., Delfosse, X., et al. 1999, A&A, 351, 619
Gaia Collaboration, Prusti, T., de Bruijne, J. H. J., et al. 2016, A&A, 595, A1
Gaia Collaboration, Brown, A. G. A., Vallenari, A., et al. 2018, A&A, 616, A1
Gaia Collaboration, Brown, A. G. A., Vallenari, A., et al. 2018, A&A, in prep.
Hartkopf, W. I., Mason, B. D., & Worley, C. E. 2001, AJ, 122, 3472. doi:10.1086/323921
Heintz, W. D. 1994, AJ, 108, 2338. doi:10.1086/117247
Henden, A. A., Templeton, M., Terrell, D., et al. 2016, VizieR Online Data Catalog, II/336
Henry, T. J., Jao, W.-C., Subasavage, J. P., et al. 2006, AJ, 132, 2360
Henry, T. J., Jao, W.-C., Winters, J. G., et al. 2018, AJ, 155, 265
Henry, T. J., Jao, W., Paredes, L. A., et al. 2021, AAS Meeting Abstracts, Meeting 237, 333.05
Horch, E. P., van Altena, W. F., Demarque, P., et al. 2015, AJ, 149, 151. doi:10.1088/0004-6256/149/5/151
Houdebine, E. R. & Mullan, D. J. 2015, ApJ, 801, 106. doi:10.1088/0004-637X/801/2/106
Izmailov, I. S. 2019, Astronomy Letters, 45, 30. doi:10.1134/S106377371901002X
Janson, M., Hormuth, F., Bergfors, C., et al. 2012, ApJ, 754, 44. doi:10.1088/0004-637X/754/1/44
Janson, M., Bergfors, C., Brandner, W., et al. 2014, ApJS, 214, 17. doi:10.1088/0067-0049/214/2/17
Jao, W.-C., Henry, T. J., Subasavage, J. P., et al. 2003, AJ, 125, 332. doi:10.1086/345515
Jao, W.-C., Henry, T. J., Subasavage, J. P., et al. 2005, AJ, 129, 1954
Jao, W.-C., Henry, T. J., Subasavage, J. P., et al. 2011, AJ, 141, 117. doi:10.1088/0004-6256/141/4/117
Jao, W.-C., Henry, T. J., Subasavage, J. P., et al. 2014, AJ, 147, 21. doi:10.1088/0004-6256/147/1/21
Jao, W.-C., Henry, T. J., Gies, D. R., et al. 2018, ApJL, 861, L11. doi:10.3847/2041-8213/aacdf6
Jeffers, S. V., Schöfer, P., Lamert, A., et al. 2018, A&A, 614, A76. doi:10.1051/0004-6361/201629599
Jódar, E., Pérez-Garrido, A., Díaz-Sánchez, A., et al. 2013, MNRAS, 429, 859. doi:10.1093/mnras/sts382
Karmakar, S., Rajpurohit, A. S., Allard, F., et al. 2020, MNRAS, 498, 737. doi:10.1093/mnras/staa2173
Kervella, P., Mérand, A., Ledoux, C., et al. 2016, A&A, 593, A127. doi:10.1051/0004-6361/201628631
Kervella, P., Arenou, F., Mignard, F., et al. 2019, A&A, 623, A72. doi:10.1051/0004-6361/201834371
Koen, C., Kilkenny, D., van Wyk, F., et al. 2010, MNRAS, 403, 1949. doi:10.1111/j.1365-2966.2009.16182.x
Köhler, R., Ratzka, T., & Leinert, C. 2012, A&A, 541, A29. doi:10.1051/0004-6361/201118707
Konopacky, Q. M., Ghez, A. M., Barman, T. S., et al. 2010, ApJ, 711, 1087. doi:10.1088/0004-637X/711/2/1087
Kratter, K. M., Matzner, C. D., Krumholz, M. R., et al. 2010, ApJ, 708, 1585. doi:10.1088/0004-637X/708/2/1585
Kroupa, P. 2008, The Cambridge N-Body Lectures, 181. doi:10.1007/978-1-4020-8431-7_8
Kuffmeier, M., Calcutt, H., & Kristensen, L. E. 2019, A&A, 628, A112. doi:10.1051/0004-6361/201935504
Lee, A. T., Offner, S. S. R., Kratter, K. M., et al. 2019, ApJ, 887, 232. doi:10.3847/1538-4357/ab584b
Lee, Y.-N., Offner, S. S. R., Hennebelle, P., et al. 2020, SSRv, 216, 70
Lurie, J. C., Henry, T. J., Jao, W.-C., et al. 2014, AJ, 148, 91. doi:10.1088/0004-6256/148/5/91
Mann, A. W., Dupuy, T., Kraus, A. L., et al. 2019, ApJ, 871, 63. doi:10.3847/1538-4357/aaf3bc
Martín, E. L., Koresko, C. D., Kulkarni, S. R., et al. 2000, ApJL, 529, L37. doi:10.1086/312450
Mason, B. D., Gies, D. R., Hartkopf, W. I., et al. 1998, AJ, 115, 821. doi:10.1086/300234
Mason, B. D., Wycoff, G. L., Hartkopf, W. I., et al. 2001, AJ, 122, 3466. doi:10.1086/323920
Mason, B. D., Hartkopf, W. I., Miles, K. N., et al. 2018, AJ, 155, 215. doi:10.3847/1538-3881/aab9b8
Moe, M. & Di Stefano, R. 2017, ApJS, 230, 15. doi:10.3847/1538-4365/aa6fb6
Moe, M., Kratter, K. M., & Badenes, C. 2019, ApJ, 875, 61. doi:10.3847/1538-4357/ab0d88
Offner, S. S. R., Dunham, M. M., Lee, K. I., et al. 2016, ApJL, 827, L11. doi:10.3847/2041-8205/827/1/L11
Oppenheimer, R., Golimowski, D. A., Kulkarni, S. R., et al. 2001, AJ, 121, 2189. doi:10.1086/319941
Pringle, J. E. 1989, MNRAS, 239, 361. doi:10.1093/mnras/239.2.361

Raghavan, D., McAlister, H. A., Henry, T. J., et al. 2010, ApJS, 190, 1. doi:10.1088/0067-0049/190/1/1
Reiners, A., Joshi, N., & Goldman, B. 2012, AJ, 143, 93. doi:10.1088/0004-6256/143/4/93
Riedel, A. R., Subasavage, J. P., Finch, C. T., et al. 2010, AJ, 140, 897. doi:10.1088/0004-6256/140/3/897
Riedel, A. R., Finch, C. T., Henry, T. J., et al. 2014, AJ, 147, 85
Riedel, A. R., Silverstein, M. L., Henry, T. J., et al. 2018, AJ, 156, 49
Scardia, M., Prieur, J.-L., Pansecchi, L., et al. 2019, Inf. Circ. 198, 1
Ségransan, D., Delfosse, X., Forveille, T., et al. 2000, A&A, 364, 665
Shan, Y., Yee, J. C., Bowler, B. P., et al. 2017, ApJ, 846, 93. doi:10.3847/1538-4357/aa859d
Söderhjelm, S. 1999, A&A, 341, 121
Tokovinin, A., Mason, B. D., & Hartkopf, W. I. 2010, AJ, 139, 743. doi:10.1088/0004-6256/139/2/743
Tokovinin, A., Mason, B. D., Hartkopf, W. I., et al. 2015, AJ, 150, 50. doi:10.1088/0004-6256/150/2/50
Tokovinin, A. 2016, Zenodo
Tokovinin, A., Cantarutti, R., Tighe, R., et al. 2016, PASP, 128, 125003. doi:10.1088/1538-3873/128/970/125003
Tokovinin, A. 2017, AJ, 154, 110. doi:10.3847/1538-3881/aa8459
Tokovinin, A. 2018, Inf. Circ. 194, 1
Tokovinin, A. 2018, PASP, 130, 035002
Tokovinin, A. 2018, Inf. Circ. 195, 1
Tokovinin, A., Mason, B. D., Mendez, R. A., et al. 2019, AJ, 158, 48. doi:10.3847/1538-3881/ab24e4
Tokovinin, A. 2019, Inf. Circ. 199, 1
Tokovinin, A. 2020, Inf. Circ. 201, 1
Tokovinin, A., Mason, B. D., Mendez, R. A., et al. 2020, AJ, 160, 7
Tokovinin, A., Mason, B. D., Mendez, R. A., et al. 2021, AJ, 162, 41. doi:10.3847/1538-3881/ac00bd
Tuomi, M., Jones, H. R. A., Barnes, J. R., et al. 2014, MNRAS, 441, 1545. doi:10.1093/mnras/stu358
Udry, S., Mayor, M., Delfosse, X., et al. 2000, IAU Symposium, 158
van de Kamp, P. 1967, San Francisco: Freeman
van Leeuwen, F. 2007, A&A, 474, 653
Vrijmoet, E. H., Henry, T. J., Jao, W.-C., & Dieterich, S. B. 2020, 160, 215
Vrijmoet, E. H., Henry, T., Tokovinin, A., et al. 2021, AAS Meeting Abstracts, Meeting 237, 530.02
Ward-Duong, K., Patience, J., De Rosa, R. J., et al. 2015, MNRAS, 449, 2618. doi:10.1093/mnras/stv384
Weis, E. W. 1996, AJ, 112, 2300. doi:10.1086/118183
Winters, J. G., Henry, T. J., Lurie, J. C., et al. 2015, AJ, 149, 5. doi:10.1088/0004-6256/149/1/5
Winters, J. G., Sevrinsky, R. A., Jao, W.-C., et al. 2017, AJ, 153, 14
Winters, J. G., Henry, T. J., Jao, W.-C., et al. 2019, AJ, 157, 216
Zechmeister, M., Kürster, M., & Endl, M. 2009, A&A, 505, 859. doi:10.1051/0004-6361/200912479
Zirm, H. 2003, IAU Commission on Double Stars, 151, 1

Table 1. Target list for the SOAR speckle program for 25 pc M dwarfs.

R.A. J2000.0 (1)	Decl. J2000.0 (2)	WDS (3)[a]	Discov. code (4)	Name (5)	π (mas) (6)	π ref. (7)[b]	V (mag) (8)	V ref. (9)	$V-K$ (mag) (10)[c]	0.9m PB (11)[d]	Lit. mult. (12)[d]	DR2 sus. (13)[d]	SOAR res. (14)[e]	Orbit ref. (15)[f]
00 06 39.24	−07 05 35.9	00067−0706	JNN 11	2MA0006-0705AB	46.960 ± 0.403	EDR3	14.72	APdr9	5.76		✓	✓	N, T2	
00 08 53.92	+20 50 25.6	00089+2050	BEU 1	G131-026AB	55.256 ± 0.761	DR2	13.52	Rie14	5.51	✓	✓	✓	Y	T3
00 09 45.04	−42 01 39.3	00098−4202		LEHPM1-0255AB	60.889 ± 0.350	EDR3	13.62	Win15	5.40			✓	Y, T2	
00 13 46.60	−04 57 37.2	00138−0458		LHS1042	42.627 ± 0.219	EDR3	17.98	estim	7.50			✓	N, T2	
00 15 27.99	−16 08 01.8	00155−1608	HEI 299	GJ1005AB	169.522 ± 0.969	Vri20	11.48	Win15	5.09	✓	✓	✓	Y	Ben16
00 15 58.07	−16 36 57.6	00160−1637	BWL 2	2MA0015-1636AB	56.096 ± 0.093	EDR3	13.20	Win19	5.29		✓	✓	Y	T3
00 16 01.97	−48 15 39.1	00160−4816	TOK 808	L290-072AB	40.672 ± 0.525	EDR3	11.55	Koe10	4.44		✓	✓	Y	
00 16 14.63	+19 51 37.5	00162+1952		GJ1006AC	65.108 ± 0.041	EDR3	12.26	Wei96	5.17		✓	✓	Y, T2	
00 21 37.26	−46 05 33.4	00216−4606		L290-028	51.569 ± 0.045	EDR3	12.24	Koe10	4.79			✓	N, T2	
00 24 44.19	−27 08 24.2	00247−2653	LEI 1AB	GJ2005AB	129.317 ± 0.126	EDR3	15.28	Win15	7.04	✓	✓	✓	Y	Koe12
00 24 44.10	−27 08 24.0	00247−2653	LEI 1BC	GJ2005BC	129.317 ± 0.126	EDR3	15.28	Win15	7.04	✓	✓	✓	Y	Man19
00 25 04.31	−36 46 17.9	00251−3646	BRG 2	LTT00220AB	49.871 ± 0.110	EDR3	12.48	Win15	4.65		✓	✓	Y	
00 27 55.99	+22 19 32.8	00279+2220	FRV 1	LP349-025AB	70.781 ± 0.427	EDR3	18.04	Win17	8.47	✓	✓	✓	Y	Dup10b
00 32 53.14	−04 34 07.0	00329−0434	JNN 12AB	GIC0050AB	52.853 ± 0.100	EDR3	13.97	Win15	5.62	✓	✓	✓	Y	
00 32 53.14	−04 34 07.0	00329−0434	JNN 12AC	GIC0050AC	52.853 ± 0.100	EDR3	13.97	Win15	5.62	✓	✓	✓	Y	
00 43 26.00	−41 17 34.0	00434−4118		LHS1134	97.661 ± 0.032	EDR3	13.00	Win15	5.29	✓			N, T2	
00 48 13.33	−05 08 07.7	00482−0508		LTT00453	40.227 ± 0.030	EDR3	12.03	Win15	4.10			✓	N, T2	
00 58 27.94	−27 51 25.4	00585−2751		GJ0046	84.979 ± 0.462	EDR3	11.77	Bes90	4.88			✓	N, T2	
01 00 56.37	−04 26 56.6	01009−0427		GJ1025	80.788 ± 0.039	EDR3	13.35	Jao05	5.13	✓			N, T2	
01 10 22.88	−67 26 41.9	01104−6727	GKI 3	GJ0054AB	121.449 ± 1.193	DR2	9.82	Hen06	4.69	✓	✓	✓	Y	Ben16
01 11 25.42	+15 26 21.5	01114+1526	BEU 2	LP467-016AB	45.79 ± 1.78	Rie14	14.46	Rie14	6.25		✓	✓	Y	
01 13 16.43	−54 29 13.8	01133−5429		DEN0113-5429	56.553 ± 0.021	EDR3	14.16	Win15	5.48	✓			N, T2	
01 22 10.33	+22 09 02.7	01222+2209	CRC 44	G034-023AB	85.68 ± 1.71	Vri20	13.03	*	5.49		✓	✓	Y	
01 28 39.51	−14 58 04.7	01287−1458		SCR0128-1458AB	74.896 ± 0.233	EDR3	13.60	Win19	5.40	✓	✓	✓	Y, T2	
01 39 01.38	−17 57 02.4	01388−1758	LDS 838	GJ0065AB	367.712 ± 0.742	EDR3	12.06	Bes91	6.72	✓	✓	✓	Y	Ker16
01 39 21.72	−39 36 09.0	01394−3936		LP991-084	114.604 ± 0.040	EDR3	14.48	Win15	6.21	✓			N, T2	
01 46 36.84	−08 38 57.6	01466−0839	JOD 3	L870-044AB	39.103 ± 1.046	DR2	12.99	Wei99	5.00	✓	✓	✓	Y	
01 47 42.50	−48 36 05.3	01477−4836		LEHPM1-1882AB	64.088 ± 0.194	EDR3	12.42	Win15	4.97	✓	✓	✓	Y, T2	
01 51 04.10	−06 07 05.0	01511−0607		LHS1302	94.711 ± 0.049	EDR3	14.49	Hen06	5.94	✓			N, T2	
01 53 37.02	−66 53 33.7	01536−6654		L088-043AB	81.82 ± 3.21	Vri20	11.68	Win15	4.69			✓	Y, T2	
01 59 12.60	+03 31 11.4	01592+0330		GJ1041BC	41.867 ± 0.023	EDR3	12.32	Win19	5.20		✓		N	
02 05 04.88	−17 36 52.8	02051−1737	BEU 3	GJ0084AB	107.300 ± 0.231	EDR3	10.19	Bes90	4.53		✓		Y	Man19
02 19 10.08	−36 46 41.2	02192−3647		GJ1046AB	65.585 ± 0.091	EDR3	11.58	Win15	4.55		✓	✓	N, T2	
02 27 30.53	−19 07 40.8	02275−1908		LP770-020AB	51.874 ± 0.321	EDR3	13.22	APdr9	4.85			✓	Y, T2	
02 27 45.86	+04 25 55.7	02278+0426	A 2329	GJ0098AB	58.33 ± 1.08	HIP07	8.67	Koe10	3.56		✓	✓	Y	And07
02 34 21.19	−53 05 36.8	02344−5306		L225-057AB	50.086 ± 0.758	DR2	12.53	Win15	5.22		✓	✓	Y, T2	

Table 1 *continued on next page*

Table 1 *(continued)*

R.A. J2000.0 (1)	Decl. J2000.0 (2)	WDS (3)[a]	Discov. code (4)	Name (5)	π (mas) (6)	π ref. (7)[b]	V (mag) (8)	V ref. (9)	$V-K$ (mag) (10)[c]	0.9m PB (11)[d]	Lit. mult. (12)[d]	DR2 sus. (13)[d]	SOAR res. (14)[e]	Orbit ref. (15)[f]
02 36 32.46	−59 28 05.5	02365−5928		APM0018	99.523 ± 0.032	EDR3	14.47	Hen06	6.13	✓			N, T2	
02 45 14.32	−43 44 10.6	02452−4344	BRG 15Aa,Ab	LP993-115BC	90.177 ± 0.025	EDR3	12.69	Rie14	5.49	✓	✓	✓	Y	T3
02 53 00.89	+16 52 52.6	02530+1653		TEE0253+1652	260.988 ± 0.093	EDR3	15.14	Die14	7.55			✓	N, T2	
03 01 51.39	−16 35 36.0	03019−1633		LP771-095A	145.692 ± 0.024	EDR3	11.22	Hen06	4.72	✓			N	
03 01 51.08	−16 35 31.1	03019−1633	RST2292BC	LP771-095BC	145.692 ± 0.024	EDR3	11.37	Hen06	5.08	✓	✓	✓	Y	Win19
03 07 55.75	−28 13 11.0	03079−2813		GJ1054AC	51.009 ± 0.019	EDR3	10.24	Wei93	3.87		✓		N, T2	
03 14 18.16	−23 09 29.8	03143−2309		LP831-045AB	62.901 ± 0.050	EDR3	12.58	Win15	4.95	✓	✓		N, T2	
03 14 51.31	−62 41 41.8	03149−6242	DAM1299	UPM0314-6241AB	37.880 ± 0.050	EDR3	12.39	APdr9	4.75		✓	✓	Y	
03 19 29.16	−30 59 44.1	03195−3060		LTT01578AB	39.022 ± 0.476	EDR3	14.00	Rei02	5.22			✓	Y, T2	
03 34 39.63	−04 50 33.4	03347−0451		LHS1561AB	37.820 ± 0.611	EDR3	13.07	Rie10	5.14		✓	✓	Y, T2	
03 35 59.70	−44 30 45.7	03360−4431		GJ1061	272.162 ± 0.032	EDR3	13.09	Lur14	6.48	✓			N, T2	
03 42 29.43	+12 31 33.6	03425+1232		LHS0178	36.712 ± 0.184	EDR3	12.87	Jao17	3.99			✓	N, T2	
03 43 22.06	−09 33 50.7	03434−0934		LHS1582AB	49.647 ± 0.254	DR2	14.69	Lur14	5.84	✓	✓	✓	N, T2	Vri20
03 52 41.75	+17 01 04.2	03527+1701		LHS1610AB	103.501 ± 0.088	EDR3	13.85	Hen18	5.80	✓	✓	✓	N, T2	
03 54 20.09	−14 37 38.6	03543−1438		DEN0354-1437AB	56.205 ± 0.663	EDR3	18.01	*	7.68			✓	Y, T2	
04 07 20.48	−24 29 13.6	04073−2429	BEU 5	LHS1630AB	54.179 ± 0.048	EDR3	12.38	Rie10	4.94	✓	✓	✓	Y	
04 08 55.60	−31 28 53.9	04089−3129	NSN 207	LP889-037AB	55.326 ± 0.023	EDR3	14.56	Win15	5.74		✓		Y	
04 09 15.67	−53 22 25.3	04093−5322		GJ0163	66.071 ± 0.012	EDR3	11.84	Bes90	4.70	✓			N, T2	
04 10 28.12	−53 36 08.1	04105−5336		GJ1068	140.696 ± 0.021	EDR3	13.60	Win15	5.70	✓			N, T2	
04 15 49.05	−46 02 23.6	04158−4602		UPM0415-4602AB	51.970 ± 0.092	EDR3	11.85	APdr9	4.56			✓	Y, T2	
04 16 41.68	−12 33 23.1	04167−1233	HDS 544	GJ2033AB	45.931 ± 0.286	EDR3	11.28	Win19	4.55		✓	✓	Y	
04 17 34.58	−48 34 39.1	04176−4835		LEHPM1-3719	60.517 ± 0.182	EDR3	15.91	*	6.57			✓	N, T2	
04 20 12.55	−70 05 58.6	04202−7006		SCR0420-7005	60.571 ± 0.042	EDR3	17.09	Win11	6.84	✓			N, T2	
04 24 11.57	−23 56 36.3	04242−2357		2MA0424-2356	64.870 ± 0.025	EDR3	12.12	APdr9	4.65			✓	N, T2	
04 29 18.47	−31 23 56.8	04293−3124	SIG 4	2MA0429-3123AB	58.794 ± 0.142	EDR3	17.39	Hos15	7.62	✓	✓	✓	Y	
04 31 09.04	−13 30 52.5	04312−1331	HDS 586	LP715-051AB	53.479 ± 0.019	EDR3	11.54	Koe10	4.49		✓		N	
04 32 42.63	−39 47 12.1	04327−3947		LHS1678	50.340 ± 0.015	EDR3	12.48	Win15	4.22	✓			N, T2	
04 35 16.15	−16 06 57.3	04353−1607		LP775-031AB	94.305 ± 0.210	EDR3	17.70	Die14	8.35	✓	✓	✓	N, T2	
04 40 29.27	−09 11 46.4	04406−0912	WOR 17	HIP021765AB	49.429 ± 0.043	EDR3	10.26	Koe10	3.99		✓		Y	Tok20b
04 46 51.78	−11 16 47.7	04469−1117	JNN 28	2MA0446-1116AB	52.772 ± 0.032	EDR3	12.25	Rie18	4.96		✓		Y	
04 48 47.39	+10 03 02.7	04488+1003		LEP0448+1003AB	57.896 ± 0.397	EDR3	12.09	APdr9	4.78		✓	✓	Y, T2	
04 52 04.02	−10 58 22.0	04521−1058		LP716-010AB	59.113 ± 0.495	EDR3	16.24	Win15	6.63			✓	Y, T2	
04 52 24.41	−16 49 21.9	04524−1649		LP776-025	63.132 ± 0.025	EDR3	11.63	Win15	4.74	✓			N, T2	
05 01 58.80	+09 58 59.0	05020+0959	HDS 654	LP476-207AB	41.039 ± 0.030	EDR3	11.53	Rie14	5.16	✓	✓		Y	
05 02 28.47	−21 15 24.0	05025−2115	DON 91AB	GJ0185AB	119.574 ± 0.042	EDR3	8.28	Win15	3.68		✓	✓	Y	Tok15c
05 06 49.47	−21 35 03.3	05069−2135	DON 93BC	BD-21-01074BC	50.523 ± 0.065	EDR3	11.08	Rie14	4.97	✓	✓	✓	Y	Tok20b
05 08 35.04	−18 10 19.4	05086−1810	WSI 72	GJ0190AB	108.325 ± 0.098	EDR3	10.31	Win15	5.00	✓	✓		Y	Tok17b
05 10 09.67	−72 36 27.9	05102−7236	WSI 122	HD271076AB	45.91 ± 2.79	Rie18	11.36	Rie18	4.31		✓	✓	Y	Tok20a
05 17 22.91	−35 21 54.6	05174−3522	TSN 1	L449-001AB	85.452 ± 0.290	EDR3	11.69	Rie14	5.13	✓	✓	✓	Y	

Table 1 *continued on next page*

Table 1 *(continued)*

R.A. J2000.0 (1)	Decl. J2000.0 (2)	WDS (3)[a]	Discov. code (4)	Name (5)	π (mas) (6)	π ref. (7)[b]	V (mag) (8)	V ref. (9)	$V-K$ (mag) (10)[c]	0.9m PB (11)[d]	Lit. mult. (12)[d]	DR2 sus. (13)[d]	SOAR res. (14)[e]	Orbit ref. (15)[f]
05 25 41.67	−09 09 12.5	05257−0909	DAE 2	LP717-036AB	46.197 ± 0.137	EDR3	12.59	Win15	4.97		✓	✓	Y	
05 28 14.60	+02 58 14.2	05282+0258		GJ1080AB	47.507 ± 0.057	EDR3	12.81	Wei96	4.59		✓	✓	N, T2	
05 32 14.66	+09 49 14.9	05322+0949		GJ0206AB	77.136 ± 0.027	EDR3	11.55	Bes90	4.99		✓		N, T2	
05 33 28.04	−42 57 20.6	05335−4257	SYU 7	SCR0533-4257AB	95.932 ± 0.246	EDR3	12.58	Hos15	5.46	✓	✓	✓	Y	T3
05 33 44.80	+01 56 43.5	05337+0157		LTT11675	63.360 ± 0.048	EDR3	11.53	Bes90	4.67			✓	N, T2	
05 40 25.73	+24 48 07.9	05404+2448	WNO 45	GJ1083AB	97.60 ± 2.80	Dit14	14.87	Wei84	6.83		✓	✓	Y	
05 44 57.04	−21 36 55.8	05450−2137		LP837-019AB	43.416 ± 0.165	EDR3	12.31	Rei02	4.49			✓	Y, T2	
05 53 14.08	+24 15 31.1	05532+2416		GJ0220AB	47.731 ± 0.512	EDR3	10.84	Wei96	4.21		✓	✓	N, T2	
06 04 52.15	−34 33 35.8	06049−3434		APCOL	115.398 ± 0.030	EDR3	12.96	Rie11	6.09	✓			N, T2	
06 10 52.90	−43 24 20.1	06109−4324		GJ1088	89.371 ± 0.021	EDR3	12.28	Rie10	4.97	✓			N, T2	
06 11 14.65	−00 35 37.8	06112−0036		UPM0611-3433	46.022 ± 0.220	EDR3	16.04	estim	6.35			✓	N, T2	
06 24 08.52	−26 55 23.6	06241−2655		UPM0624-2655AB	49.214 ± 0.856	DR2	11.51	APdr9	4.61			✓	Y, T2	
06 24 10.12	−00 16 30.5	06242−0017		G106-045AB	45.614 ± 0.200	EDR3	14.04	APdr9	5.20			✓	Y, T2	
06 29 23.39	−02 48 48.8	06293−0248	B 2601AB	GJ0234AB	242.966 ± 0.883	DR2	11.12	Win15	5.63	✓	✓	✓	Y	Man19
06 30 46.47	−76 43 09.6	06308−7643	HEN 4	SCR0630-7643AB	112.658 ± 0.093	EDR3	14.82	Win11	6.90	✓	✓	✓	Y	
06 31 31.04	−88 11 36.6	06315−8812		SCR0631-8811AB	63.31 ± 2.07	Win17	15.65	Win11	6.58			✓	Y, T2	
06 32 20.30	−09 43 29.0	06323−0943		UPM0632-0943AB	38.388 ± 0.413	EDR3	14.48	*	5.50	✓		✓	Y, T2	
06 35 29.85	−04 03 18.4	06354−0403	JNN 271	2MA0635-0403AB	79.164 ± 0.309	EDR3	14.59	APdr9	6.28		✓	✓	Y	
06 36 18.28	−40 00 23.6	06363−4000		LP381-004AB	52.000 ± 0.188	EDR3	10.59	Koe10	3.80			✓	Y, T2	
06 39 37.41	−21 01 33.2	06396−2102		LP780-032AB	65.308 ± 0.325	EDR3	12.77	Win15	5.12			✓	Y, T2	
06 43 40.67	−26 24 41.0	06437−2625		LTT02631AB	58.141 ± 0.017	EDR3	12.92	Win15	4.79		✓		N, T2	
06 52 18.04	−05 11 24.0	06523−0510	WSI 125Ba,Bb	GJ0250BC	114.291 ± 0.022	EDR3	10.09	Wei96	4.37		✓		N	
06 57 46.62	−44 17 28.2	06579−4417	LPM 248	GJ0257AB	124.357 ± 0.040	EDR3	10.85	Koe02	4.79		✓		Y	Zir03
06 59 40.78	−56 22 47.6	06597−5623		SCR0659-5622AB	41.0 ± 8.5	Win15	14.81	Win15	5.32			✓	Y, T2	
07 02 50.33	−61 02 47.5	07028−6103		SCR0702-6102AB	57.024 ± 0.197	EDR3	16.62	Win17	7.10	✓		✓	Y, T2	
07 04 17.70	−10 30 31.6	07043−1031	BEU 9	GJ0263AB	63.551 ± 0.514	EDR3	11.30	Bes90	4.87		✓	✓	Y	Man19
07 09 37.66	−57 03 42.1	07096−5704		APM0089	58.556 ± 0.059	EDR3	13.64	Win15	5.34		(✓)		Y, T2	
07 20 03.25	−08 46 49.9	07200−0847	BUG 17	WIS0720-0846AB	148.80 ± 1.08	Hen18	18.54	Hen18	9.07	✓	✓	✓	N	Bur15b
07 23 59.62	−80 15 18.0	07240−8015		SCR0723-8015AB	61.730 ± 0.126	EDR3	17.45	Win15	7.01	✓	✓		N, T2	
07 27 24.50	+05 13 32.8	07274+0514	WDK 2	GJ0273AB	264.127 ± 0.041	EDR3	9.88	Dav15	5.02		✓	✓	N	
07 28 13.10	−18 47 35.7	07282−1848		LHS1918AB	73.969 ± 0.526	EDR3	13.69	Win21	5.52	✓	✓	✓	Y, T2	
07 28 51.37	−30 14 48.5	07289−3015	HDS1054AB	GJ2060AB	64.140 ± 0.473	EDR3	9.92	Koe10	4.20		✓	✓	Y	Tok18c
07 33 26.82	−27 49 04.1	07334−2749		SCR0733-2749AB	44.2 ± 8.7	Win15	16.03	Win15	5.95			✓	Y, T2	
07 36 25.12	+07 04 43.1	07364+0705	HEN 3	G089-032AB	117.59 ± 0.83	Hen18	13.25	Hen18	5.97	✓	✓	✓	Y	Tok18c
07 40 11.80	−42 57 40.3	07402−4258		SCR0740-4257	125.303 ± 0.022	EDR3	13.81	Win11	6.04	✓			N, T2	
07 54 54.73	−29 20 56.3	07549−2920	KUI 32	LHS1955AB	80.098 ± 0.144	EDR3	12.79	Rie10	5.44	✓	✓	✓	Y	Mas18
07 57 32.53	−71 14 53.8	07575−7115		SCR0757-7114AB	44.342 ± 0.020	EDR3	12.45	Rie14	5.03		(✓)		N, T2	
08 02 57.81	−83 30 07.5	08030−8330		GAI0802-8330AB	42.911 ± 0.277	EDR3	16.03	estim	6.32			✓	Y, T2	
08 08 16.85	−73 01 40.2	08083−7302		LEP0808-7301AC	43.371 ± 0.498	EDR3	14.05	APdr9	5.06			✓	Y, T2	

Table 1 *continued on next page*

Table 1 *(continued)*

R.A. J2000.0 (1)	Decl. J2000.0 (2)	WDS (3)[a]	Discov. code (4)	Name (5)	π (mas) (6)	π ref. (7)[b]	V (mag) (8)	V ref. (9)	$V-K$ (mag) (10)[c]	0.9m PB (11)[d]	Lit. mult. (12)[d]	DR2 sus. (13)[d]	SOAR res. (14)[e]	Orbit ref. (15)[f]
08 10 34.29	−13 48 51.1	08107−1348	JOD 4Ba,Bb	GJ0297.2BC	44.520 ± 0.049	EDR3	11.82	Wei99	4.40		✓	✓	Y	
08 11 57.56	+08 46 23.0	08120+0846		GJ0299	147.722 ± 0.095	EDR3	12.86	Dav15	5.20			✓	N, T2	
08 13 08.46	−13 55 01.1	08132−1354	HU 115A	GJ0301AB	46.559 ± 0.444	EDR3	9.37	Koe10	3.55		✓	✓	Y	Izm19
08 15 11.20	−23 44 15.6	08152−2344		UPM0815-2344AB	101.041 ± 0.027	EDR3	12.36	Hen18	5.14	✓		✓	N, T2	
08 20 13.37	+05 32 08.1	08202+0532		LEP0820+0532	44.508 ± 0.036	EDR3	11.91	APdr9	4.24			✓	N, T2	
08 22 47.41	−57 26 52.9	08228−5727	BRG 27Aa,Ab	LHS2005AB	77.632 ± 0.037	EDR3	13.39	*	5.59		✓		Y	
08 27 11.83	−44 59 21.1	08272−4459	JOD 5	LHS2010AB	72.614 ± 0.048	EDR3	11.86	Rie10	4.99		✓		N, T2	
08 31 37.43	+19 23 49.7	08317+1924	DEL 1Ba,Bb	GJ2069BD	60.249 ± 0.076	EDR3	13.37	Hos15	5.65	✓	✓	✓	Y	
08 31 37.57	+19 23 39.4	08317+1924	BEU 12Aa,Ab	GJ2069ACE	60.060 ± 0.036	EDR3	11.93	Hos15	5.33	✓	✓	✓	Y	Seg00
08 37 20.42	−28 19 57.5	08373−2820		SCR0837-2819AB	43.663 ± 0.795	EDR3	15.59	Win15	5.70			✓	Y, T2	
08 38 02.17	−58 55 58.4	08380−5856		SCR0838-5855AB	89.993 ± 0.236	EDR3	17.19	Win15	7.92	✓	✓	✓	Y, T2	
08 38 33.74	−28 43 26.3	08386−2843		UPM0838-2843AB	73.316 ± 0.036	EDR3	11.85	APdr9	4.57			✓	Y, T2	
08 42 44.53	+09 33 24.1	08427+0935	ST 8AB	GJ0319AC	64.681 ± 0.112	EDR3	9.63	Koe10	3.80		✓	✓	Y	
08 52 49.87	−66 08 47.4	08528−6609		SCR0852-6608AB	40.0 ± 7.6	Win15	16.41	Win15	6.02			✓	Y, T2	
08 54 05.33	−13 07 30.7	08539−1308	ST 9AB	GJ0326AB	64.936 ± 0.150	EDR3	11.93	Wei96	4.67		✓	✓	Y	
08 54 31.99	−05 51 25.7	08545−0551		2MA0854-0551AB	45.572 ± 0.121	EDR3	13.44	*	5.12			✓	Y, T2	
08 55 20.25	−23 52 14.6	08553−2352		LHS2071AB	64.077 ± 0.223	EDR3	13.88	Rie10	5.68	✓	✓	✓	Y, T2	Rie10
08 57 04.68	+11 38 48.8	08571+1139	HDS1296	GJ0330AB	61.324 ± 0.105	EDR3	10.57	Bes90	4.08		✓	✓	Y	Tok19c
08 58 15.07	+19 45 48.2	08582+1945	LDS3836	GJ1116AB	194.144 ± 0.123	EDR3	13.69	Win19	6.80		✓		Y	Tok20b
08 58 56.32	+08 28 26.1	08589+0829	DEL 2	G041-014AB	146.97 ± 1.51	Hen18	10.92	Hen06	5.23		✓	✓	Y	
09 01 10.48	+01 56 35.2	09012+0157	CRC 57Aa,Ab	LTT12366AC	42.633 ± 0.349	EDR3	11.84	*	4.78		✓	✓	Y	
09 15 36.40	−10 35 47.2	09156−1036	MTG 2	LHS6167AB	103.54 ± 0.77	Hen18	13.82	Win15	6.09	✓	✓	✓	Y	Mas18
09 29 03.78	−24 29 04.2	09291−2429		WT1637AB	56.66 ± 0.97	Win17	16.87	Win15	6.96			✓	Y, T2	
09 31 19.41	−13 29 18.9	09313−1329	KUI 41	GJ0352AB	99.88 ± 3.60	HIP07	10.08	Bes90	4.57		✓	✓	Y	Man19
09 31 22.32	−17 17 42.3	09314−1718		LP788-001AB	63.759 ± 0.692	EDR3	17.55	Win15	7.48	✓	✓	✓	N, T2	
09 36 57.83	−26 10 11.2	09370−2610	WSI 127AB	2MA0936-2610AB	55.352 ± 0.750	EDR3	13.12	Rie18	5.16		✓	✓	Y	Tok20b
09 42 46.34	−68 53 06.0	09428−6853		GJ1128	153.759 ± 0.025	EDR3	12.74	Lur14	5.70	✓			N, T2	
09 44 23.73	−73 58 38.3	09444−7359		WT0244AB	40.845 ± 0.245	EDR3	15.17	Rie10	5.79			✓	Y, T2	
09 44 54.19	−12 20 54.4	09449−1221		G161-071	76.051 ± 0.034	EDR3	13.76	Win15	6.16	✓			N, T2	
09 45 40.08	−39 02 26.7	09457−3902	HDS1409	LP462-119AB	50.593 ± 0.315	EDR3	12.11	Win19	4.59		✓	✓	Y	Tok18c
09 45 58.43	−32 53 30.0	09460−3254		WT2458	83.250 ± 0.037	EDR3	14.04	Win15	5.76	✓		✓	N, T2	
09 50 40.54	−13 48 38.6	09507−1349		LP728-070AB	51.14 ± 1.86	Win17	12.71	Win15	4.99		✓	✓	Y, T2	
09 53 11.78	−03 41 24.5	09532−0341		GJ0372AB	63.612 ± 0.074	EDR3	10.55	Bes90	4.42		✓		N, T2	
09 55 23.86	−27 15 40.7	09554−2716		LP847-048	91.737 ± 0.039	EDR3	12.08	Win15	4.94			✓	N, T2	
09 58 34.32	−46 25 30.4	09586−4626		GJ0375AB	64.719 ± 0.020	EDR3	11.27	Win15	5.01	✓	✓		N, T2	
10 06 52.10	−12 46 54.4	10069−1247		2MA1006-1246AB	46.8 ± 4.9	Fin18	14.51	*	5.61			✓	Y, T2	
10 12 04.67	−02 41 05.2	10121−0241	DEL 3	GJ0381AB	86.659 ± 0.701	DR2	10.64	Bes90	4.45		✓	✓	Y	Tok18a
10 14 51.77	−47 09 24.2	10149−4709		LHS0281	79.321 ± 0.018	EDR3	13.49	Jao05	5.17	✓			N, T2	
10 17 26.90	−53 54 26.5	10174−5354	CVN 16Aa,Ab	TWA022AB	50.521 ± 0.199	EDR3	14.05	Win19	6.36		✓	✓	Y	Tok19c

Table 1 *continued on next page*

Table 1 *(continued)*

R.A. J2000.0 (1)	Decl. J2000.0 (2)	WDS (3)[a]	Discov. code (4)	Name (5)	π (mas) (6)	π ref. (7)[b]	V (mag) (8)	V ref. (9)	$V-K$ (mag) (10)[c]	0.9m PB (11)[d]	Lit. mult. (12)[d]	DR2 sus. (13)[d]	SOAR res. (14)[e]	Orbit ref. (15)[f]
10 19 53.71	−41 48 59.8	10199−4149		L392-039BC	43.402 ± 0.017	EDR3	13.17	Win17	4.88			✓	Y, T2	
10 36 44.84	+15 21 39.9	10367+1522	DAE 3AB	2MA1036+1521AB	49.979 ± 0.089	EDR3	13.33	Win19	5.43		✓	✓	Y	Cal17
10 36 44.92	+15 21 38.0	10367+1522	DAE 3BC	2MA1036+1521BC	49.979 ± 0.089	EDR3	13.33	Win19	5.43		✓	✓	Y	Cal17
10 39 44.35	−37 55 13.5	10397−3755	HDS1523	LP465-084AB	71.51 ± 2.48	HIP07	11.08	Win15	4.70		✓	✓	Y	Tok20b
10 41 09.34	−36 53 43.5	10412−3654	HDS1528	GJ1135AB	62.624 ± 0.145	EDR3	9.94	Koe10	3.95		✓		Y	
10 42 41.36	−24 16 04.1	10427−2416		LP848-050AB	96.149 ± 0.469	DR2	16.53	Win17	7.19	✓	✓	✓	N, T2	
10 43 02.86	−09 12 40.9	10430−0913	WSI 112	WT1827AB	82.001 ± 0.286	EDR3	15.11	Win15	7.38	✓	✓	✓	Y	
10 48 12.62	−11 20 09.6	10482−1120		LHS0292	219.330 ± 0.060	EDR3	15.78	Die14	7.85	✓			N, T2	
10 48 14.57	−39 56 06.8	10482−3956		DEN1048-3956	247.216 ± 0.051	EDR3	17.37	Lur14	8.92	✓		✓	N, T2	
10 54 41.96	−07 18 33.4	10547−0719	CRC 62	LTT04004AB	48.807 ± 0.201	EDR3	13.29	Win15	5.32	✓	✓	✓	Y	
10 55 15.31	−73 56 09.0	10553−7356		WIS1055-7356	77.499 ± 0.477	EDR3	17.54	estim	7.87			✓	N, T2	
10 56 28.83	+07 00 53.3	10565+0701		GJ0406	415.179 ± 0.068	EDR3	13.58	Die14	7.50	✓		✓	N, T2	
10 58 05.31	−55 25 17.6	10581−5525		GAI1058-5525AB	50.421 ± 0.100	EDR3	15.72	estim	6.14			✓	Y, T2	
11 30 41.83	−08 05 43.0	11307−0806		LP672-042	74.205 ± 0.025	EDR3	12.06	Win15	4.91	✓			N/A	
11 31 08.39	−14 57 21.3	11311−1457		LHS0306	86.900 ± 0.048	EDR3	14.19	Win15	5.69	✓		✓	N, T2	
11 35 26.95	−32 32 23.9	11354−3232		GJ0433	110.171 ± 0.020	EDR3	9.84	Bes90	4.22	✓			N, T2	
12 06 58.53	−35 00 52.0	12070−3501		SCR1206-3500AB	40.757 ± 0.165	EDR3	14.67	Win11	5.54			✓	Y, T2	
12 10 42.16	−22 13 06.0	12107−2213	... ...	2MA1210-2213BC	52.834 ± 0.029	EDR3	13.06	APdr9	4.54			✓	Y	
12 14 16.56	+00 37 26.4	12143+0037		GJ1154AB	123.643 ± 0.045	EDR3	13.66	Dav15	6.12		✓		N, T2	
12 20 05.10	−18 12 59.5	12201−1813		LP794-053AB	39.641 ± 0.256	EDR3	15.60	*	5.98			✓	Y, T2	
12 20 33.68	−82 25 57.5	12206−8226		NLTT30359AB	81.749 ± 0.608	DR2	11.96	Win15	5.12	✓	✓	✓	Y, T2	
12 28 57.60	+08 25 31.1	12290+0826	WSI 113	GJ0469AB	72.266 ± 0.696	EDR3	12.05	Hos15	5.09	✓	✓	✓	Y	Ben16
12 29 34.54	−55 59 37.0	12296−5560		GJ1158	76.353 ± 0.022	EDR3	13.26	Jao11	5.19	✓		✓	N, T2	
12 30 01.73	−34 11 24.1	12300−3411		SCR1230-3411AB	52.556 ± 0.263	EDR3	14.16	Win11	5.73	✓	✓	✓	Y, T2	Win17
12 33 17.36	+09 01 15.8	12335+0901	REU 1	GJ0473AB	231.119 ± 0.512	EDR3	12.47	Ben16	6.43	✓	✓	✓	Y	Sca19
12 33 33.08	−48 26 11.4	12336−4826		L327-121AB	48.090 ± 0.781	DR2	12.07	Win15	4.93	✓	✓	✓	Y, T2	
12 35 58.40	−45 56 20.5	12360−4556		GJ0477AB	48.210 ± 0.596	DR2	11.12	Bes90	4.28		✓	✓	N, T2	
12 41 08.05	−38 43 12.9	12411−3843		SIP1241-3843AB	42.845 ± 0.275	EDR3	17.65	estim	7.20			✓	Y, T2	
12 43 59.05	−16 14 35.5	12440−1615		LP796-001AB	51.3 ± 3.4	Fin18	14.75	*	5.85			✓	Y, T2	
12 50 52.65	−21 21 13.6	12509−2121		LEHPM2-0174	56.788 ± 0.188	EDR3	18.36	Die14	8.23	✓		✓	N, T2	
12 56 02.15	−12 57 21.7	12560−1257	SJM 1Aa,Ab	LP736-015AB	47.273 ± 0.473	EDR3	17.76	*	7.72		✓	✓	Y	
13 00 46.56	+12 22 32.7	13008+1223	BEU 16AB	GJ0494AB	86.901 ± 0.117	EDR3	9.73	Bes90	4.15		✓		N	Hei94
13 13 09.32	−41 30 39.8	13132−4131		ER2	84.314 ± 0.447	EDR3	12.90	Win15	5.49	✓		✓	Y, T2	
13 14 20.38	+13 20 01.0	13143+1320	LAW 2	NLTT33370AB	61.0 ± 2.8	Lep09	15.88	Win19	7.09		✓	✓	Y	Dup16
13 16 45.41	−12 20 20.4	13168−1220		LP737-014AB	44.797 ± 0.554	EDR3	13.65	APdr9	5.01			✓	Y, T2	
13 23 38.03	−25 54 45.1	13236−2555		LHS2729	71.119 ± 0.039	EDR3	12.89	Rie14	5.11	✓			N, T2	
13 24 46.48	−05 04 19.9	13248−0504		G014-052AB	40.562 ± 0.323	EDR3	13.88	Win15	5.32			✓	Y, T2	
13 28 21.08	−02 21 37.1	13283−0222		GJ0512A	75.878 ± 0.057	EDR3	11.35	Win15	4.74			✓	N, T2	
13 28 21.50	−02 21 31.7	13283−0222		GJ0512B	75.595 ± 0.440	EDR3	13.69	Bes90	5.39			✓	N, T2	

Table 1 *continued on next page*

Table 1 *(continued)*

R.A. J2000.0 (1)	Decl. J2000.0 (2)	WDS (3)[a]	Discov. code (4)	Name (5)	π (mas) (6)	π ref. (7)[b]	V (mag) (8)	V ref. (9)	$V-K$ (mag) (10)[c]	0.9m PB (11)[d]	Lit. mult. (12)[d]	DR2 sus. (13)[d]	SOAR res. (14)[e]	Orbit ref. (15)[f]
13 42 09.83	−16 00 23.3	13422−1600	WSI 114	LHS2783AB	49.458 ± 0.073	EDR3	13.42	Win15	5.33		✓	✓	Y	
13 58 05.41	−39 37 55.1	13581−3938		SSS1358-3938	86.541 ± 0.026	EDR3	14.04	Win15	5.09	✓			N, T2	
14 04 08.18	−66 14 38.1	14041−6615		NLTT36064AB	61.860 ± 0.461	EDR3	11.59	Win15	4.67			✓	Y, T2	
14 11 59.91	−41 32 22.1	14120−4132	MTG 3	WT0460AB	109.732 ± 0.232	EDR3	15.65	Win15	7.03	✓	✓	✓	Y	
14 12 10.97	−00 35 04.5	14121−0035	WSI 129Aa,Ab	LHS2875AB	37.030 ± 0.166	EDR3	13.04	Bes91	4.49		✓	✓	Y	
14 15 32.55	+04 39 31.4	14155+0440		GJ1182AB	72.004 ± 0.367	EDR3	14.30	Wei96	5.68		✓	✓	N, T2	
14 20 36.83	−75 16 05.7	14206−7516		SCR1420-7516	40.832 ± 0.186	EDR3	13.78	Win11	5.15			✓	Y, T2	
14 29 42.95	−62 40 46.1	14396−6050		PROXIMA	768.067 ± 0.050	EDR3	11.13	Lur14	6.75			✓	N, T2	
14 34 04.88	−18 24 10.7	14341−1824		LHS5273AB	36.770 ± 0.316	EDR3	14.35	*	5.64			✓	Y, T2	
14 34 16.81	−12 31 10.4	14343−1231		GJ0555	159.923 ± 0.055	EDR3	11.34	Win15	5.40	✓			N, T2	
14 44 06.56	−34 26 47.1	14441−3427		SCR1444-3426	65.044 ± 0.032	EDR3	14.17	Win11	5.29	✓			N, T2	
14 53 51.40	+23 33 21.0	14540+2335	REU 2	GJ0568AB	86.276 ± 0.186	EDR3	11.68	Wei96	5.11		✓		Y	Mas18
14 54 10.43	−20 41 28.4	14542−2042		LP801-025AB	43.190 ± 0.335	EDR3	15.03	*	5.69			✓	Y, T2	
14 54 29.42	+16 06 08.6	14545+1606	MEL 2Ba,Bb	GJ0569BC	100.524 ± 0.021	EDR3	17.16	estim	11.39		✓	✓	N, T2	Kon10
14 57 26.53	−21 24 41.6	14575−2125	H N 28Ba,Bb	GJ0570BC	169.884 ± 0.065	EDR3	8.07	Koe10	4.27		✓		Y	For99
15 09 31.95	−15 46 47.8	15095−1547		GAI1509-1546AB	31.132 ± 0.063	EDR3	12.21	APdr9	4.14			✓	Y, T2	
15 15 43.71	−07 25 21.2	15157−0725		G151-037AB	57.144 ± 0.123	EDR3	12.93	Win17	5.22			✓	Y, T2	
15 19 11.73	−12 45 06.3	15192−1245	CRC 72	LHS3056AB	46.440 ± 0.318	EDR3	12.87	Win15	5.29		✓	✓	Y	
15 19 26.83	−07 43 20.2	15194−0743		GJ0581	158.718 ± 0.030	EDR3	10.56	Lur14	4.72			✓	N, T2	
15 24 48.49	−49 29 47.5	15248−4930		L264-018	45.767 ± 0.290	EDR3	11.64	APdr9	4.34		✓	✓	N, T2	
15 30 52.05	−68 01 17.8	15309−6801		NLTT40317AB	50.482 ± 0.194	EDR3	13.52	Win15	5.29			✓	Y, T2	
15 31 54.16	+28 51 09.6	15319+2851		LHS3080AB	37.638 ± 0.686	EDR3	14.32	Rie10	5.50	✓	✓	✓	Y, T2	
15 42 06.54	−19 28 18.3	15421−1928		GJ0595AB	103.180 ± 0.316	EDR3	11.84	Win15	4.67	✓	✓	✓	N, T2	Hen18
15 45 41.61	−43 30 28.4	15457−4330		LTT06288AB	47.932 ± 0.140	EDR3	13.06	Win15	4.98	✓	✓	✓	Y, T2	Vri20
15 46 41.69	−55 34 47.5	15467−5535		SCR1546-5534AB	119.096 ± 0.703	DR2	17.58	Win15	8.47	✓	✓	✓	Y, T2	
15 47 24.55	−10 53 47.3	15474−1054		LHS3117AB	62.516 ± 0.277	DR2	11.28	Koe10	4.54		✓	✓	Y, T2	
15 47 29.81	−27 55 12.1	15475−2755	GAT 18AB	UPM1547-2755AB	40.192 ± 0.030	EDR3	13.08	APdr9	4.61		✓		Y	
15 47 34.90	−27 53 42.9	15476−2754		UPM1547-2755CD	40.673 ± 0.395	EDR3	16.71	estim	6.36			✓	Y, T2	
15 57 50.42	−51 31 49.0	15578−5132		GAI1557-5131AB	59.719 ± 0.271	DR2	16.93	estim	7.26			✓	Y, T2	
16 01 56.10	−33 57 11.9	16019−3357		LP553-044AB	66.086 ± 0.234	EDR3	12.17	Rei04	5.24			✓	Y, T2	
16 16 58.94	−31 36 37.6	16170−3137		GAI1616-3136AB	54.544 ± 0.301	DR2	14.04	APdr9	5.56			✓	Y, T2	
16 20 03.21	−37 31 48.6	16202−3734		GJ0618B	117.679 ± 0.107	EDR3	14.15	Bes90	6.38			✓	N/A	
16 20 03.51	−37 31 44.4	16202−3734		GJ0618A	117.472 ± 0.029	EDR3	10.59	Koe10	4.64		✓		N, T2	
16 26 48.14	−17 23 34.2	16268−1724	WSI 131	LHS3197AB	55.661 ± 0.260	EDR3	14.30	Rie10	5.62		✓	✓	Y	
16 26 51.68	−38 12 32.6	16269−3813		SCR1626-3812	71.737 ± 0.049	EDR3	15.75	Win15	6.31	✓			N, T2	
16 30 13.09	−14 39 49.5	16302−1440	WSI 132	GJ2121AB	44.161 ± 0.159	EDR3	12.35	Wei96	4.75		✓	✓	Y	Tok20a
16 30 27.30	−36 33 56.8	16305−3634	WSI 133	SCR1630-3633AB	59.474 ± 0.036	EDR3	14.93	obsli	5.90		✓		Y	
16 45 16.93	−38 48 33.5	16453−3848	RST1900Aa,Ab	GJ2122AB	67.233 ± 0.241	EDR3	9.68	Hos15	3.96	✓	✓	✓	Y	
16 50 57.94	+22 27 05.7	16510+2227		G169-029	95.520 ± 0.026	EDR3	14.08	Win17	5.77	✓			N/A	

Table 1 *continued on next page*

Table 1 *(continued)*

R.A. J2000.0 (1)	Decl. J2000.0 (2)	WDS (3)[a]	Discov. code (4)	Name (5)	π (mas) (6)	π ref. (7)[b]	V (mag) (8)	V ref. (9)	$V-K$ (mag) (10)[c]	0.9m PB (11)[d]	Lit. mult. (12)[d]	DR2 sus. (13)[d]	SOAR res. (14)[e]	Orbit ref. (15)[f]
16 55 28.76	−08 20 10.8	16555−0820	KUI 75AB	GJ0644AB	155.43 ± 0.49	Vri20	9.03	Bes90	4.63		✓	✓	Y	Sod99
16 58 25.21	+13 58 10.8	16584+1358	YSC 61	G139-003AB	70.90 ± 2.06	Win17	13.16	Win17	5.19		✓	✓	Y	
17 07 40.85	+07 22 06.7	17077+0722	YSC 62	GJ1210AB	82.00 ± 2.30	Dit14	14.02	Wei96	5.60		✓	✓	Y	Mas18
17 10 44.33	−53 00 25.6	17107−5300	NSN 374	UPM1710-5300AB	45.777 ± 0.052	EDR3	12.12	Win15	4.96		✓		Y	
17 11 52.25	−01 51 06.3	17119−0151	LPM 629	GJ0660AB	98.19 ± 12.09	HIP07	11.37	Bes90	4.71		✓	✓	Y	Doc19
17 12 51.28	−05 07 31.4	17129−0508		GJ0660.1A	43.259 ± 0.356	EDR3	11.61	Bes90	3.67			✓	N, T2	
17 13 40.47	−08 25 14.8	17137−0825		GJ1212AB	48.484 ± 0.329	EDR3	12.03	Koe10	4.78		✓	✓	Y, T2	
17 17 44.09	+11 40 12.4	17177+1140		GJ1215AB	80.841 ± 0.145	EDR3	15.10	Wei96	6.17	✓	✓	✓	N, T2	Dah88
17 18 21.71	−01 46 53.4	17184−0147	BAG 51	HIP084652AB	45.030 ± 0.191	EDR3	10.59	Wei93	3.87		✓	✓	Y	
17 18 58.83	−34 59 48.6	17190−3459		GJ0667C	138.066 ± 0.028	EDR3	10.34	Lur14	4.30				N	
17 28 11.05	−01 43 57.3	17282−0144		SCR1728-0143AB	37.375 ± 0.391	EDR3	14.42	Win15	5.41			✓	Y, T2	
17 29 46.20	−25 03 53.6	17298−2504		LP864-014AB	55.391 ± 0.806	DR2	13.55	APdr9	5.09			✓	Y, T2	
17 33 40.66	−42 55 42.3	17337−4256	GAT 23	GAI1733-4255AB	44.786 ± 0.104	EDR3	13.96	estim	5.28		✓	✓	Y	
17 36 31.17	−25 15 00.9	17365−2515		GAI1736-2515AB	60.239 ± 0.831	DR2	16.39	estim	8.50			✓	Y, T2	
17 37 03.67	−44 19 09.2	17371−4419	WDK 3	GJ0682AB	199.694 ± 0.031	EDR3	10.99	Win15	5.38	✓	✓		N, T2	
17 43 00.80	+05 47 21.6	17430+0547	HDS2506	G140-009AB	47.828 ± 0.657	EDR3	10.67	Wei86	4.04		✓	✓	Y	Tok19c
17 46 14.42	−32 06 08.4	17462−3206		GJ2130BC	70.734 ± 0.116	EDR3	11.51	Ben16	4.92		✓	✓	N, T2	
17 46 34.23	−57 19 08.7	17466−5719		GJ0693	169.804 ± 0.047	EDR3	10.77	Win15	4.75	✓			N, T2	
17 57 48.50	+04 41 36.1	17578+0441		BARNARDS	546.976 ± 0.040	EDR3	9.54	Dav15	5.02			✓	N/A	
18 03 36.04	−18 58 49.9	18036−1859		G154-043AB	75.604 ± 0.681	EDR3	14.13	Win15	5.85	✓	✓	✓	Y, T2	
18 09 43.70	−02 19 35.1	18097−0220		LSR1809-0219	61.245 ± 0.453	DR2	15.10	Win15	5.83			✓	N, T2	
18 09 51.97	−10 27 13.3	18099−1027		UPM1809-1027AB	31.326 ± 0.383	EDR3	13.12	*	5.00			✓	Y, T2	
18 11 15.25	−78 59 22.9	18113−7859	KPP3056	L043-072AB	85.634 ± 0.462	EDR3	12.57	Win15	5.61		✓	✓	Y	
18 20 57.16	−01 02 58.0	18210−0101	VKI 46	GJ1226AB	56.265 ± 0.045	EDR3	13.07	Jao05	5.12		✓	✓	Y	
18 26 46.83	−65 42 40.0	18268−6543		SCR1826-6542AB	66.40 ± 0.73	Win17	17.35	Win11	7.80		✓	✓	N, T2	
18 38 44.75	−14 29 26.0	18387−1429	HDS2641AB	GJ2138AB	74.792 ± 0.053	EDR3	11.22	Koe10	4.37		✓		N	
18 41 09.76	+24 47 14.4	18411+2447		GJ1230AC	100.685 ± 0.022	EDR3	12.32	Win19	5.70		✓		N, T2	
18 45 05.25	−63 57 47.5	18451−6358	BIL 1	SCR1845-6357AB	249.665 ± 0.133	EDR3	17.40	Win11	8.89	✓	✓	✓	N/A	
18 45 57.46	−28 55 53.7	18460−2856		LTT07434AB	53.207 ± 0.647	EDR3	12.68	Win15	5.08	✓	✓	✓	Y, T2	
18 48 20.97	−68 55 34.4	18483−6856	JAO 8	SCR1848-6855AB	43.924 ± 0.098	EDR3	16.86	Jao14	5.76	✓	✓	✓	N, T2	Jao14
18 55 27.41	+08 24 09.0	18555+0824		GJ0735AB	89.907 ± 0.026	EDR3	10.12	Bes90	4.69		✓		N, T2	
18 59 40.71	−63 27 22.1	18597−6327		L159-126AB	60.426 ± 1.512	DR2	13.05	*	4.97			✓	Y, T2	
19 12 14.62	+02 53 11.4	19121+0254	AST 1	GJ0748AB	106.279 ± 1.063	DR2	11.10	Lur14	4.81	✓	✓	✓	Y	Ben16
19 12 39.25	−36 14 56.6	19127−3615		WIS1912-3615	87.084 ± 0.072	EDR3	13.91	Win15	5.14			✓	N, T2	
19 13 07.97	−39 01 53.9	19131−3902	WSI 135	LHS3443AB	46.936 ± 0.026	EDR3	12.39	Rie10	4.73		✓	✓	Y	
19 20 47.98	−45 33 29.6	19208−4534		GJ0754	169.235 ± 0.059	EDR3	12.25	Win15	5.40	✓		✓	N, T2	
19 21 38.70	+20 52 03.3	19216+2052		GJ1235	94.399 ± 0.043	EDR3	13.48	Hen18	5.54			✓	N, T2	
19 24 10.93	−09 31 33.5	19242−0932		SCR1924-0931AB	27.540 ± 0.454	EDR3	13.89	Win15	4.96			✓	Y, T2	
19 27 52.71	−28 11 15.8	19279−2811	WJG 6	LHS5348AB	66.218 ± 0.070	EDR3	14.85	Win15	6.06		✓	✓	Y	

Table 1 *continued on next page*

Table 1 *(continued)*

R.A. J2000.0 (1)	Decl. J2000.0 (2)	WDS (3)[a]	Discov. code (4)	Name (5)	π (mas) (6)	π ref. (7)[b]	V (mag) (8)	V ref. (9)	$V-K$ (mag) (10)[c]	0.9m PB (11)[d]	Lit. mult. (12)[d]	DR2 sus. (13)[d]	SOAR res. (14)[e]	Orbit ref. (15)[f]
19 31 01.40	−73 37 05.2	19310−7337		LEP1931-7337AB	51.687 ± 0.092	EDR3	12.89	APdr9	4.65			✓	Y, T2	
19 34 03.95	−52 25 14.1	19341−5225		L275-026	54.510 ± 0.029	EDR3	12.83	Win15	4.91	✓			N, T2	
19 42 00.65	−21 04 05.4	19420−2104		LP869-019AB	53.582 ± 0.047	EDR3	13.22	Win15	5.40		✓		N, T2	
19 43 24.58	−37 22 10.1	19434−3722	BRG 29	2MA1943-3722AB	41.387 ± 0.028	EDR3	13.68	*	5.43		✓	✓	Y	
19 44 53.81	−23 38 00.2	19449−2338	MTG 4	LP869-026AB	67.388 ± 0.175	EDR3	14.09	Win15	5.82		✓	✓	Y	Mas18
19 46 50.51	−01 57 39.6	19468−0158		LEP1946-0157	42.588 ± 0.409	EDR3	12.14	APdr9	4.39			✓	N, T2	
19 51 35.83	−35 10 37.5	19516−3511	NSN 488	2MA1951-3510AB	88.207 ± 0.075	EDR3	13.06	Win15	5.32		✓		Y	
19 51 40.39	−31 00 22.2	19517−3100		UPM1951-3100AB	76.440 ± 0.860	DR2	12.28	*	4.87	✓	✓	✓	Y, T2	
19 54 24.88	−31 47 59.8	19544−3148		LP926-055AB	41.277 ± 0.438	EDR3	13.07	*	4.75			✓	Y, T2	
20 15 22.68	−56 45 54.5	20154−5646		L209-071AC	41.371 ± 0.290	EDR3	12.85	Win15	5.08	✓		✓	Y, T2	
20 25 18.95	−22 59 06.0	20253−2259		SCR2025-2259AB	14.123 ± 0.633	EDR3	14.22	Win11	5.06			✓	Y, T2	
20 29 48.32	+09 41 20.6	20298+0941	AST 2AB	GJ0791.2AB	133.811 ± 1.387	DR2	13.13	Win19	5.82	✓	✓	✓	Y	Tok19b
20 33 01.89	−49 03 11.1	20330−4903		LEHPM2-1265AB	55.510 ± 0.536	DR2	15.33	Win15	6.14	✓	✓	✓	N	
20 49 09.96	−40 12 06.0	20492−4012		SCR2049-4012AB	105.156 ± 0.266	DR2	13.53	Hos15	5.83	✓	✓	✓	Y, T2	Hen18
20 55 37.74	−14 02 08.1	20556−1402		LHS0501AC	84.856 ± 0.471	EDR3	12.48	Jao11	5.11	✓	✓	✓	Y, T2	T3
21 01 07.40	−49 07 25.1	21011−4907		WT0766AC	74.455 ± 0.761	EDR3	13.35	Sub17	5.16		✓	✓	N, T2	
21 14 12.20	−76 33 25.3	21142−7633		2MA2114-7633AB	51.210 ± 0.081	EDR3	12.23	APdr9	4.99			✓	Y, T2	
21 17 34.09	−44 44 34.5	21176−4445		2MA2117-4444AB	55.889 ± 0.087	EDR3	14.02	APdr9	5.49			✓	Y, T2	
21 20 09.80	−67 39 05.6	21202−6739		L117-123	47.022 ± 0.306	EDR3	10.90	Koe10	4.07			✓	N, T2	
21 28 18.28	−22 18 32.4	21283−2219		L714-046	47.325 ± 0.028	EDR3	12.17	Win15	4.54			✓	N, T2	
21 29 36.80	+17 38 35.9	21296+1739		GJ0829AB	147.496 ± 0.026	EDR3	10.30	Wei91	4.85		✓		Y, T2	
21 30 47.67	−40 42 29.5	21308−4043		LHS0510	82.092 ± 0.028	EDR3	13.12	Win15	4.99	✓			N, T2	
21 31 18.57	−09 47 26.5	21313−0947	BLA 9	GJ0831AB	134.083 ± 1.113	DR2	12.02	Win15	5.64	✓	✓	✓	Y	Ben16
21 34 22.30	−43 16 10.6	21344−4316		WT0792	59.021 ± 0.033	EDR3	16.38	Win15	6.69	✓			N, T2	
21 36 25.30	−44 01 00.1	21364−4401		WT0795	70.492 ± 0.033	EDR3	14.15	Rie10	5.62	✓			N, T2	
21 38 43.65	−33 39 55.2	21387−3340		LHS0512	82.678 ± 0.045	EDR3	12.55	Win15	4.98	✓			N, T2	
21 39 00.93	−24 09 29.3	21390−2409		GJ0836AB	51.399 ± 0.071	EDR3	13.45	Bes90	5.09	✓		✓	N, T2	
21 49 05.76	−72 06 09.1	21491−7206	HEI 598	GJ1264AB	60.776 ± 0.069	EDR3	9.62	Koe10	3.97		✓	✓	Y	Tok20b
21 49 11.31	−41 33 28.7	21492−4133		L427-034A	65.399 ± 0.453	EDR3	13.14	Win17	6.26			✓	N	
21 49 44.83	−41 38 32.8	21497−4139		WT0818AB	38.623 ± 0.589	EDR3	13.56	Win15	5.02	✓		✓	Y, T2	
21 55 48.36	−33 13 14.8	21558−3313		LP983-034AB	42.999 ± 0.485	EDR3	12.73	APdr9	5.03			✓	Y, T2	
21 56 55.25	−01 54 09.3	21569−0154		LHS0516	74.220 ± 0.037	EDR3	14.65	Wei96	5.62	✓			N, T2	
21 58 49.12	−32 26 25.6	21588−3226		LHS3739BC	55.686 ± 0.633	EDR3	15.78	Lur14	6.02	✓	✓	✓	N, T2	Lur14
22 01 49.05	+16 28 02.8	22018+1628	YSC 165	GJ0844AB	61.79 ± 2.23	HIP07	10.65	Koe10	4.47		✓	✓	Y	Man19
22 02 29.38	−37 04 51.4	22025−3705		LHS3746	130.419 ± 0.053	EDR3	11.76	Hen06	5.04	✓		✓	N, T2	
22 06 40.69	−44 58 07.5	22067−4458		WT0870AB	56.561 ± 0.138	EDR3	14.43	Rie10	5.54			✓	Y, T2	
22 16 40.67	−48 00 36.4	22167−4801		SCR2216-4800AB	36.371 ± 0.205	EDR3	13.66	*	5.06			✓	Y, T2	
22 17 18.70	−08 48 19.3	22173−0847	BEU 22Ba,Bb	GJ0852BC	90.489 ± 0.222	EDR3	14.43	Wei96	5.90		✓		Y	
22 17 19.23	−34 44 03.5	22173−3444		LP984-001AB	51.503 ± 0.088	EDR3	15.48	Win15	6.31			✓	Y, T2	

Table 1 *continued on next page*

Table 1 *(continued)*

R.A. J2000.0 (1)	Decl. J2000.0 (2)	WDS (3)[a]	Discov. code (4)	Name (5)	π (mas) (6)	π ref. (7)[b]	V (mag) (8)	V ref. (9)	$V-K$ (mag) (10)[c]	0.9m PB (11)[d]	Lit. mult. (12)[d]	DR2 sus. (13)[d]	SOAR res. (14)[e]	Orbit ref. (15)[f]
22 23 07.00	−17 36 26.3	22231−1736		LHS3799	138.228 ± 0.048	EDR3	13.30	Rie14	5.98	✓			N, T2	
22 28 23.24	−25 54 10.6	22284−2553	LDS2944AB	LP876-026AC	42.417 ± 0.024	EDR3	13.36	*	5.85		✓	✓	Y	
22 28 23.42	−25 54 07.7	22284−2553	WSI 137Aa,Ab	LP876-026AB	42.417 ± 0.024	EDR3	12.45	*	5.00		✓	✓	Y	
22 30 09.41	−53 44 55.5	22302−5345		LEHPM1-4771AB	64.358 ± 0.389	EDR3	14.47	Win15	5.84	✓	✓	✓	Y, T2	Vri20
22 35 04.89	−42 17 48.0	22351−4218		LTT09084AB	66.2 ± 10.5	Win15	13.34	Win15	5.13		✓	✓	Y, T2	
22 36 09.69	−00 50 29.8	22360−0050	JOD 25AB	GJ0864AB	60.384 ± 0.041	EDR3	9.99	Bes90	3.83		✓		Y	
22 38 29.75	−65 22 42.6	22384−6523	HDS3215	GJ0865AB	76.33 ± 1.44	Vri20	11.48	Bes90	5.05		✓	✓	Y	Tok18c
22 38 33.58	−15 17 59.8	22385−1519	BLA 10AB	GJ0866AB	293.600 ± 0.900	Tor10	12.37	Bes90	6.83		✓	✓	Y	Seg00
22 38 45.28	−20 36 51.8	22388−2037		GJ0867BD	112.987 ± 0.039	EDR3	11.45	Bes90	4.96		✓		N, T2	
22 38 45.57	−20 37 16.1	22388−2037		GJ0867AC	112.386 ± 0.056	EDR3	9.09	Bes90	4.29		✓		N, T2	
22 48 38.39	−31 08 40.7	22486−3109		LP932-081	49.663 ± 0.737	EDR3	12.33	Win15	4.84			✓	N, T2	
23 03 35.60	−46 50 47.0	23036−4651	WSI 139	SCR2303-4650AB	67.359 ± 0.855	EDR3	13.89	Win17	5.53	✓	✓	✓	Y	Tok20b
23 05 52.04	−35 51 11.1	23059−3551		GJ0887AB	304.135 ± 0.020	EDR3	7.34	Bes90	3.87		✓		N, T2	
23 07 19.88	−04 15 32.8	23073−0416		2MA2307-0415AC	48.356 ± 0.234	EDR3	10.73	APdr9	3.99			✓	Y, T2	
23 08 19.55	−15 24 35.8	23083−1525		GJ0890	40.100 ± 0.024	EDR3	10.84	Bes90	3.73		(✓)		Y, T2	
23 10 42.16	−19 13 34.4	23107−1914		GJ1281	46.822 ± 0.061	EDR3	12.45	Jao05	4.22	✓		✓	N, T2	
23 11 57.79	−17 01 58.8	23120−1702		LP822-037AB	53.2 ± 14.4	Win15	13.95	*	5.25			✓	Y, T2	
23 24 11.31	−17 45 50.3	23242−1746		G273-033AB	43.881 ± 0.381	EDR3	11.93	APdr9	4.17			✓	Y, T2	
23 25 24.90	−67 40 07.2	23254−6740		SCR2325-6740AB	31.63 ± 1.53	Vri20	14.38	Win11	5.33			✓	Y, T2	
23 30 13.44	−20 23 27.4	23302−2023		GJ1284AB	62.868 ± 0.076	EDR3	11.14	Rie14	4.81		✓		N, T2	
23 36 52.30	−36 28 51.7	23369−3629		LHS0547	83.676 ± 0.023	EDR3	13.76	Jao05	5.34	✓			N, T2	
23 45 31.28	−16 10 19.4	23455−1610	MTG 5	LHS4009AB	79.97 ± 1.37	Rie10	14.38	Rie10	6.07		✓	✓	Y	Man19
23 48 36.06	−27 39 38.9	23486−2740		LHS4016AB	38.233 ± 0.040	EDR3	12.34	Rie14	4.60		✓		N, T2	
23 52 23.47	−14 41 24.3	23524−1441		LHS4032AB	39.108 ± 0.483	EDR3	15.30	Wei96	5.75			✓	Y, T2	
23 54 50.21	−09 57 01.1	23548−0957		LP763-082AB	38.920 ± 0.146	EDR3	12.19	Rei03	4.50			✓	Y, T2	
23 55 39.78	−06 08 33.4	23557−0609		GJ0912AB	55.920 ± 0.044	EDR3	11.16	Bes90	4.44		(✓)		Y, T2	
23 57 19.36	−12 58 40.7	23573−1259	BWL 67Aa,Ab	LP704-014AC	50.413 ± 0.067	EDR3	12.98	Wei91	4.75		✓		Y	
23 58 32.66	+07 39 30.1	23585+0740		LTT17066AB	59.094 ± 0.278	EDR3	11.71	Wei86	4.65			✓	Y, T2	
23 59 44.77	−44 05 00.3	23597−4405	WSI 140	LTT09828AB	58.267 ± 0.530	DR2	12.81	Win15	4.77	✓	✓	✓	Y	Vri20

Table 1 *continued on next page*

Table 1 *(continued)*

R.A. J2000.0 (1)	Decl. J2000.0 (2)	WDS (3)[a]	Discov. code (4)	Name (5)	π (mas) (6)	π ref. (7)[b]	V (mag) (8)	V ref. (9)	$V-K$ (mag) (10)[c]	0.9m PB (11)[d]	Lit. mult. (12)[d]	DR2 sus. (13)[d]	SOAR res. (14)[e]	Orbit ref. (15)[f]

References— * = This work, APdr9 = Henden et al. (2016), And07 = Andrade (2007), Ben16 = Benedict et al. (2016), Bur15b = Burgasser et al. (2015), Cal17 = Calissendorff et al. (2017), Dah88 = Dahn et al. (1988), Dit14 = Dittmann et al. (2014), Doc19 = Docobo et al. (2019), Dup10b = Dupuy et al. (2010), Dup16 = Dupuy et al. (2016), For99 = Forveille et al. (1999), EDR3 = *Gaia* EDR3 (Gaia Collaboration et al. 2020), DR2 = *Gaia* DR2 (Gaia Collaboration et al. 2018), Hei94 = Heintz (1994), Hen18 = Henry et al. (2018), HIP07 = van Leeuwen (2007), Izm19 = Izmailov (2019), Jao14 = Jao et al. (2014), Ker16 = Kervella et al. (2016), Koe10 = Koen et al. (2010), Koe12 = Köhler et al. (2012), Kon10 = Konopacky et al. (2010), Lur14 = Lurie et al. (2014), Man19 = Mann et al. (2019), Mas18 = Mason et al. (2018), Rie10 = Riedel et al. (2010), Rie14 = Riedel et al. (2014), Rie18 = Riedel et al. (2018), Seg00 = Ségransan et al. (2000), Sca19 = Scardia et al. (2019), Sod99 = Söderhjelm (1999), Tok15c = Tokovinin et al. (2015), Tok17b = Tokovinin (2017), Tok18a = Tokovinin (2018a), Tok18c = Tokovinin (2018c), Tok19c = Tokovinin et al. (2019a), Tok19b = Tokovinin (2019b), Tok20a = Tokovinin (2020a), Tok20b = Tokovinin et al. (2020b), Vri20 = Vrijmoet et al. (2020), Wei96 = Weis (1996), Win15 = Winters et al. (2015), Win17 = Winters et al. (2017), Win19 = Winters et al. (2019), Zir03 = Zirm (2003)

[a] Column 3 — For all systems not already noted in the WDS catalog (Mason et al. 2001), the WDS code given is the anticipated code for the future entry should these systems be resolved.

[b] Column 7 — The parallax reference is "EDR3" for *Gaia* EDR3 (Gaia Collaboration et al. 2020), "DR2" for DR2 (Gaia Collaboration et al. 2018), or other references as listed in the Table notes.

[c] Column 10 — Reference for all K magnitudes in $V-K$ color is (Cutri et al. 2003).

[d] Columns 11–13 — These are classification flags indicating the subsets to which each system belongs: 0.9 m PB = system with perturbation in RECONS astrometry residuals (§2.1), Lit. mult. = known binary from the literature (§2.2), DR2 sus. = system with evidence of multiplicity in *Gaia* DR2 results (§2.3). Check marks in parentheses (✓) in column 12 indicate unpublished results from coauthor Winters (to be published speckle survey results).

[e] Column 14 — This column indicates SOAR resolutions and non-resolutions as presented in previous papers in the yearly SOAR series (e.g., Tokovinin et al. 2019a, 2020b, 2021), except those noted with the "T2" flag, which are given in Table 2.

[f] Column 15 — This column gives the reference for the existing orbit in the literature from the Sixth Catalog of Orbits of Visual Binary Stars (Hartkopf et al. 2001), with flag "T4" noting orbits newly presented in this work in Table 4 and Figure 2.

Table 2. Results of observations through 2020 in the SOAR speckle program for 25 pc M dwarfs. All magnitude differences are in the I band, except where the y band is noted in column 11.

WDS (1)[a]	First res. (2)[b]	Date obs. (year) (3)	Resol. (Y/N) (4)	ρ ($''$) (5)[c]	θ (deg) (6)[c]	Δm (mag) (7)[c]	$\rho_{\rm min}$ ($''$) (8)[d]	Δm ($0.''15$) (mag) (9)[d]	Δm ($1.''0$) (mag) (10)[d]	Obs. flags (11)[e]
00067−0706	Jan14	2019.8568	N				0.0768	2.3	2.9	
		2020.8342	N				0.0594	2.3	2.8	
00098−4202	*	2019.6133	Y	0.0522	159.0	0.8				
		2019.8567	N				0.0525	2.5	3.9	
		2020.8341	Y	0.0959	115.7	1.0				
		2020.9270	Y	0.1089	117.4	0.9				q
00138−0458	none	2019.8568	N				0.1145	1.6	2.5	:
		2020.8342	N				0.1260	1.6	1.6	:
00162+1952	*	2019.5397	N				0.0636	2.3	3.9	
		2019.8564	N				0.0543	2.7	4.1	
		2020.9241	Y	0.0312	44.8	1.0				
00216−4606	none	2019.9523	N				0.0415	3.3	4.3	
		2020.9270	N				0.0415	2.8	5.2	
00434−4118	none	2019.6133	N				0.0492	2.5	4.0	
		2019.8567	N				0.0470	2.8	4.3	
		2020.8341	N				0.0508	2.7	4.1	
00482−0508	none	2019.9495	N				0.0415	2.4	4.8	
		2020.8342	N				0.0477	2.9	4.2	
00585−2751	none	2019.5369	N				0.0463	2.7	4.2	
		2019.8568	N				0.0444	2.6	4.1	
		2020.9271	N				0.0415	2.9	5.2	
01009−0427	none	2019.5397	N				0.0562	2.5	4.2	
		2019.8568	N				0.0543	2.8	3.7	
		2020.8365	N				0.0463	2.6	4.0	
01133−5429	none	2020.1110	N				0.0643	2.3	3.3	
		2020.8365	N				0.0562	2.5	3.2	
01287−1458	*	2018.5621	Y	0.4115	338.7	2.6				q
		2019.6134	Y	0.3686	326.5	2.6				q
		2020.8344	Y	0.3241	307.8	2.6				q
		2020.9271	Y	0.3205	306.2	2.7				q
01394−3936	none	2019.5370	N				0.0508	2.5	3.9	
		2020.8344	N				0.0500	2.5	3.9	
01477−4836	*	2019.5370	Y	0.5562	30.6	0.6				p
		2019.8567	Y	0.5482	28.5	0.6				q
		2020.8365	Y	0.5095	22.6	0.6				q
01511−0607	none	2019.5399	N				0.0670	2.3	3.7	
		2019.8568	N				0.0553	2.5	3.5	
		2020.8367	N				0.0508	2.7	4.0	
01536−6654	**	2019.6132	N				0.0485	2.8	4.2	
		2019.8567	N				0.0508	2.6	4.2	
		2020.8368	Y	0.0914	245.5	3.0				
02192−3647	none	2019.5370	N				0.0437	2.4	3.8	
		2019.9498	N				0.0415	3.1	5.4	
02275−1908	**	2019.5398	Y	0.2249	196.2	1.8				q
		2019.8593	Y	0.2068	201.4	1.8				
		2020.8345	Y	0.1179	232.4	1.8				q
02344−5306	*	2019.5344	Y	0.1504	312.0	0.1				
		2019.8567	Y	0.1357	330.9	0.1				
		2019.9470	Y	0.1314	337.1	0.1				

Table 2 *continued on next page*

Table 2 *(continued)*

WDS (1)[a]	First res. (2)[b]	Date obs. (year) (3)	Resol. (Y/N) (4)	ρ ($''$) (5)[c]	θ (deg) (6)[c]	Δm (mag) (7)[c]	$\rho_{\rm min}$ ($''$) (8)[d]	Δm ($0\farcs15$) (mag) (9)[d]	Δm ($1\farcs0$) (mag) (10)[d]	Obs. flags (11)[e]
		2020.8344	Y	0.1122	59.2	0.1				
		2020.9243	Y	0.1149	68.2	0.1				
02365−5928	none	2019.5345	N				0.0562	2.6	3.7	
		2019.8568	N				0.0553	2.5	3.5	
		2020.8368	N				0.0534	2.6	3.6	
02530+1653	none	2019.9496	N				0.0420	0.0	3.3	
		2020.8369	N				0.0516	2.8	3.9	
03079−2813	none	2019.8593	N				0.0432	2.7	4.0	
		2020.8236	N				0.0432	2.7	4.4	
03143−2309	none	2019.8593	N				0.0485	2.6	4.1	
		2020.8236	N				0.0463	2.8	4.1	
03195−3060	*	2019.6136	Y	0.5501	133.0	1.3				q
		2019.8593	Y	0.5573	132.1	1.2				p
		2020.9269	Y	0.5804	129.8	1.3				:
03347−0451	*	2018.8409	Y	0.0977	218.5	0.9				q
		2018.9747	Y	0.1034	211.6	1.0				q
		2019.6136	Y	0.1365	188.3	0.9				q
		2019.8571	Y	0.1430	181.1	0.9				q
		2020.0182	Y	0.1401	176.6	0.9				
		2020.8236	Y	0.1140	151.5	0.9				q
		2020.9243	Y	0.1077	146.0	0.9				q
03360−4431	none	2019.6135	N				0.0636	2.7	4.7	
		2019.8594	N				0.0477	2.8	4.1	
		2020.8368	N				0.0492	2.9	4.4	
03425+1232	none	2018.7317	N				0.0525	2.1	3.3	
		2019.8569	N				0.0759	2.2	3.9	
03434−0934	none	2018.9724	N				0.0415	1.4	4.3	
		2020.8236	N				0.0534	2.4	3.3	
03527+1701	none	2019.8569	N				0.0553	2.5	3.7	
		2020.8369	N				0.0534	2.5	3.9	
03543−1438	**	2019.8571	Y	0.1875	130.8	0.4				:
		2020.8369	Y	0.1963	117.1	1.0				:
04093−5322	none	2019.6136	N				0.0636	2.7	4.6	
		2020.1111	N				0.0463	2.4	3.8	
04158−4602	**	2019.6136	Y	0.7318	84.6	0.5				p
		2019.8594	Y	0.7270	83.5	0.4				p
		2020.1111	Y	0.7199	82.8	0.5				p
04176−4835	none	2019.6138	N				0.0716	2.6	4.0	
		2019.8594	N				0.0716	2.1	3.7	
		2020.9271	N				0.0573	2.2	3.0	
04202−7006	none	2019.9469	N				0.0415	2.2	4.3	
		2020.8286	N				0.1068	1.8	2.6	:
04242−2357	none	2019.9500	N				0.0415	3.0	5.5	
		2020.8237	N				0.0450	2.7	4.2	
04327−3947	none	2019.8594	N				0.0470	2.8	4.1	
		2019.9500	N				0.0415	2.4	4.9	
		2020.0182	N				0.0415	2.8	4.3	
		2020.8369	N				0.0500	2.8	4.0	
04353−1607	none	2019.8571	N				0.0670	2.3	3.6	
		2020.8237	N				0.0606	2.1	2.9	
04488+1003	*	2019.9498	Y	0.1075	302.5	0.4				q
		2020.1111	Y	0.0885	316.7	0.5				
		2020.8346	Y	0.0784	91.3	0.3				q

Table 2 *continued on next page*

Table 2 *(continued)*

WDS (1)[a]	First res. (2)[b]	Date obs. (year) (3)	Resol. (Y/N) (4)	ρ ($''$) (5)[c]	θ (deg) (6)[c]	Δm (mag) (7)[c]	$\rho_{\rm min}$ ($''$) (8)[d]	Δm ($0\farcs15$) (mag) (9)[d]	Δm ($1\farcs0$) (mag) (10)[d]	Obs. flags (11)[e]
		2020.9244	Y	0.0824	103.0	0.3				
04521−1058	**	2019.8571	Y	0.2393	51.3	2.6				
		2020.1111	Y	0.2390	42.3	2.9				
		2020.8237	Y	0.2443	31.9	2.8				
04524−1649	none	2020.1110	N				0.0437	2.5	3.7	
		2020.9271	N				0.0415	2.7	5.7	
05282+0258	none	2019.9471	N				0.0415	2.7	4.9	
		2019.7914	N				0.0677	2.6	4.3	
		2019.8571	N				0.0534	2.5	3.9	
		2020.9272	N				0.0415	3.1	5.0	
05322+0949	none	2019.7914	N				0.0636	2.7	4.7	
		2019.8571	N				0.0463	2.5	3.7	
		2020.9272	N				0.0415	2.7	5.5	
05337+0157	none	2019.9471	N				0.0415	2.3	5.5	
		2020.8373	N				0.0470	2.7	4.3	
05450−2137	**	2019.8595	Y	0.1665	24.2	0.2				
		2019.9497	Y	0.1632	22.8	0.1				
		2020.1112	Y	0.1568	20.5	0.0				
		2020.8370	Y	0.1113	5.0	0.2				
05532+2416	none	2019.8600	N				0.0492	2.5	4.1	
		2020.9274	N				0.0415	2.8	4.7	
06049−3434	none	2019.8595	N				0.0477	2.5	4.4	
		2020.8370	N				0.0492	2.9	4.3	
06109−4324	none	2020.1112	N				0.0450	2.6	4.0	
		2020.9271	N				0.0415	3.0	5.2	
06112−0036	none	2019.8596	N				0.0955	2.1	3.1	
		2020.8373	N				0.0656	1.8	2.6	:
06241−2655	**	2019.8595	Y	0.1618	29.7	0.5				q
		2019.9524	Y	0.1569	26.1	0.4				
		2020.8372	Y	0.0559	294.3	0.3				q
		2020.9244	Y	0.0538	267.3	0.5				
06242−0017	**	2019.8599	Y	0.0248	36.4	0.2				
		2019.9473	N				0.0458	2.0	4.0	
		2020.1115	Y	0.0453	108.2	0.4				
		2020.8373	Y	0.0954	133.4	0.0				
		2020.9246	Y	0.1014	136.4	0.0				
06315−8812	*	2019.9469	Y	0.1195	330.8	0.6				q
		2020.0183	Y	0.1331	330.5	0.8				:
		2020.8346	Y	0.0757	348.2	0.0				:
06323−0943	*	2019.1993	Y	0.2043	61.9	0.3				
		2019.8596	Y	0.2180	62.0	0.4				q
		2020.1115	Y	0.2254	62.0	0.4				q
		2020.8372	Y	0.2372	62.2	0.4				
06363−4000	**	2019.8597	Y	0.1782	73.2	2.3				q
		2019.9524	Y	0.1720	73.7	2.3				q
		2020.8372	Y	0.0858	79.7	2.1				
06396−2102	*	2019.8596	Y	0.5306	249.7	0.3				
		2020.1115	Y	0.5301	252.1	0.1				q
		2020.8372	Y	0.5303	259.1	0.2				q
06437−2625	none	2019.8596	N				0.0477	2.4	3.8	
		2020.8372	N				0.0508	2.5	3.9	
06597−5623	**	2019.8571	Y	0.2314	142.4	0.0				
		2020.1111	Y	0.2326	141.4	0.1				

Table 2 *continued on next page*

Table 2 *(continued)*

WDS (1)[a]	First res. (2)[b]	Date obs. (year) (3)	Resol. (Y/N) (4)	ρ ($''$) (5)[c]	θ (deg) (6)[c]	Δm (mag) (7)[c]	$\rho_{\rm min}$ ($''$) (8)[d]	Δm ($0.''15$) (mag) (9)[d]	Δm ($1.''0$) (mag) (10)[d]	Obs. flags (11)[e]
		2020.8374	Y	0.2321	137.5	0.0				
07028−6103	*	2019.8571	Y	0.0753	26.5	0.0				:
		2019.9475	Y	0.0776	16.2	0.4				
		2020.0182	Y	0.0928	358.1	0.2				:
		2020.1111	Y	0.0635	7.4	0.3				:
		2020.8374	Y	0.0644	12.7	0.5				:
		2020.9246	Y	0.0509	348.5	0.0				
		2020.9957	Y	0.0601	344.7	0.0				:
07096−5704	**	2019.8571	N				0.0618	2.3	3.2	
		2020.1111	N				0.0562	2.3	3.4	
		2020.9957	Y	0.0351	70.9	0.1				
07240−8015	none	2019.9469	N				0.0448	1.6	3.0	
		2020.1113	N				0.0875	1.7	2.8	:
		2020.8347	N				0.1312	1.6	1.9	:
07282−1848	*	2019.8599	Y	0.5315	210.6	1.5				q
		2020.1115	Y	0.5315	213.2	1.4				q
		2020.8373	Y	0.5300	221.0	1.5				q
07334−2749	**	2019.8599	Y	0.4295	232.9	0.2				:
		2020.1115	Y	0.4270	233.8	0.4				:
07402−4258	none	2019.8597	N				0.0492	2.7	3.9	
		2020.1116	N				0.0500	2.6	3.9	
		2020.9246	N				0.0415	2.7	5.0	
07575−7115	none	2019.8572	N				0.0562	2.6	4.0	
		2020.8346	N				0.0516	2.7	3.9	
08030−8330	**	2019.8573	Y	0.1168	152.0	0.0				:
		2019.9469	Y	0.1232	151.8	0.5				
		2020.1113	Y	0.1328	134.5	0.0				:
		2020.8346	Y	0.1373	139.2	0.0				:
08083−7302	**	2019.9528	Y	0.2798	343.5	0.5				:
		2020.1113	Y	0.2778	343.9	0.5				:
08120+0846	none	2019.9474	N				0.0415	2.4	4.8	
08152−2344	none	2019.9528	N				0.0415	2.8	4.9	
		2020.9274	N				0.0415	2.8	5.4	
08202+0532	none	2019.9474	N				0.0415	3.0	5.2	
08272−4459	Jod13	2019.8597	N				0.0470	2.6	4.1	
		2020.9274	N				0.0415	3.0	5.3	
08373−2820	**	2019.9501	Y	0.1219	246.5	0.5				q
		2020.1116	Y	0.1216	243.5	0.8				q
		2020.8374	Y	0.1055	237.4	0.7				:
08380−5856	*	2019.8572	Y	0.4781	348.7	1.7				q
		2020.1113	Y	0.4768	347.0	1.9				q
08386−2843	**	2019.9501	Y	0.0478	98.4	0.0				
		2020.1116	Y	0.0303	167.5	0.1				:
		2020.8374	Y	0.0329	148.5	0.0				
		2020.9274	Y	0.0387	90.7	0.0				
08528−6609	**	2019.9475	Y	0.2944	46.1	0.3				
		2020.1113	Y	0.2924	45.9	0.1				:
08545−0551	**	2019.9474	Y	0.1612	266.9	3.1				q
		2020.0186	Y	0.1529	268.3	3.0				
		2020.1116	Y	0.1588	267.5	3.4				
08553−2352	*	2018.2358	Y	0.4005	202.8	2.6				q
		2019.9501	Y	0.3299	219.1	2.5				q
		2020.1116	Y	0.3168	222.7	2.5				q

Table 2 *continued on next page*

Table 2 *(continued)*

WDS (1)[a]	First res. (2)[b]	Date obs. (year) (3)	Resol. (Y/N) (4)	ρ ($''$) (5)[c]	θ (deg) (6)[c]	Δm (mag) (7)[c]	$\rho_{\rm min}$ ($''$) (8)[d]	Δm ($0\farcs15$) (mag) (9)[d]	Δm ($1\farcs0$) (mag) (10)[d]	Obs. flags (11)[e]
		2020.8374	Y	0.2912	231.0	2.4				q
09291−2429	**	2019.9502	Y	0.4203	199.1	0.1				
		2020.1117	Y	0.4184	199.0	0.0				
		2020.9958	Y	0.4190	197.2	0.1				:
09314−1718	none	2019.9502	N				0.0415	1.3	3.9	
09428−6853	none	2019.9528	N				0.0415	2.7	4.2	
09444−7359	*	2019.8573	Y	0.3322	279.4	1.7				q
		2019.9530	Y	0.3284	278.1	1.5				:
09449−1221	none	2019.9502	N				0.0415	2.0	5.1	
09460−3254	none	2019.9502	N				0.0415	2.1	5.3	
09507−1349	*	2019.9502	Y	0.3552	302.6	0.0				q
		2020.1116	Y	0.3541	302.4	0.1				
09532−0341	none	2019.9502	N				0.0415	1.8	4.8	
09554−2716	none	2019.9502	N				0.0415	2.5	5.4	
		2020.9957	N				0.0470	2.4	4.3	
09586−4626	none	2019.9474	N				0.0415	2.9	5.6	
		2020.9961	N				0.0485	2.7	4.5	
10069−1247	**	2019.9503	Y	0.1801	202.5	0.0				
		2020.0184	Y	0.1883	205.7	0.0				:
10149−4709	none	2019.9528	N				0.0415	2.5	3.9	
		2020.2004	N				0.0415	2.6	4.9	
10199−4149	**	2019.9475	Y	0.1683	127.9	0.2				
		2020.0184	Y	0.1738	129.7	0.1				
		2020.9961	Y	0.2304	146.4	0.2				:
10427−2416	none	2018.2358	N				0.0600	0.0	1.8	:
		2020.9958	N				0.0670	1.8	1.9	:
10482−1120	none	2019.9503	N				0.0415	2.5	4.8	
10482−3956	none	2019.9475	N				0.0415	2.3	4.6	
10553−7356	none	2020.2006	N				0.0663	0.0	2.0	:
10565+0701	none	2019.9530	N				0.0415	2.7	4.9	
10581−5525	**	2020.1117	Y	0.0949	9.9	0.0				
		2020.9961	Y	0.0740	52.1	0.3				:
11311−1457	none	2019.9503	N				0.0415	2.0	4.9	
11354−3232	none	2019.9529	N				0.0415	2.8	5.7	
		2019.5359	N				0.0414	2.7	4.1	
12070−3501	**	2019.5359	Y	0.6156	45.9	2.0				p
		2020.0186	Y	0.6310	45.7	1.9				p
12143+0037	none	2020.0187	N				0.0415	2.7	4.6	
12201−1813	**	2019.5359	Y	0.1147	309.7	1.4				
		2020.0187	Y	0.0969	311.1	0.7				:
12206−8226	*	2019.5386	Y	0.1175	69.5	2.3				
		2020.1117	Y	0.1939	54.6	2.3				q
		2020.2006	Y	0.1981	53.0	2.2				q
12296−5560	none	2020.0188	N				0.0420	2.9	3.4	
12300−3411	*	2019.5359	Y	0.1260	56.3	2.0				q
		2020.0187	Y	0.1100	61.6	1.8				q
		2020.1171	Y	0.1003	64.0	1.7				q
12336−4826	*	2019.5333	Y	0.1151	355.8	0.4				q
		2020.0187	Y	0.1544	13.3	0.4				
		2020.1169	Y	0.1602	15.9	0.4				q
12360−4556	none	2019.5333	N				0.0477	2.7	4.2	
12411−3843	**	2019.5333	Y	0.2962	171.4	1.8				:
		2020.1171	Y	0.2992	174.0	2.2				:

Table 2 *continued on next page*

Table 2 *(continued)*

WDS	First res.	Date obs. (year)	Resol. (Y/N)	ρ ($''$)	θ (deg)	Δm (mag)	$\rho_{\rm min}$ ($''$)	Δm ($0.''15$) (mag)	Δm ($1.''0$) (mag)	Obs. flags
(1)[a]	(2)[b]	(3)	(4)	(5)[c]	(6)[c]	(7)[c]	(8)[d]	(9)[d]	(10)[d]	(11)[e]
12440−1615	**	2019.5359	Y	0.3377	88.9	0.0				
		2020.0187	Y	0.3301	85.2	0.0				
12509−2121	none	2019.5359	N				0.0969	2.0	3.4	:
		2020.1171	N				0.0875	2.0	2.7	
13132−4131	**	2019.5333	Y	0.0602	89.3	2.5				:
		2020.0188	N				0.0415	3.3	4.3	
		2020.1168	N				0.0485	2.5	4.0	
13168−1220	**	2019.5359	Y	0.1690	232.1	1.6				q
		2020.0188	Y	0.1771	241.7	1.4				
13236−2555	none	2020.0188	N				0.0415	2.9	4.3	
13248−0504	**	2019.5360	Y	0.6043	280.6	0.6				p
		2020.1173	Y	0.5978	279.4	0.4				:
13283−0222 A	none	2018.3996	N				0.0415	2.5	4.2	
		2019.5360	N				0.0477	2.2	3.4	
13283−0222 B	none	2018.3996	N				0.0475	2.6	3.2	
		2019.5360	N				0.0553	2.1	3.2	
13581−3938	none	2019.5334	N				0.0636	2.3	4.1	
		2020.1172	N				0.0508	2.4	4.1	
14041−6615	**	2019.5386	Y	0.1709	32.1	3.9				
		2020.1118	N				0.0492	2.4	4.2	
		2020.2006	N				0.0415	2.4	5.5	
14155+0440	none	2019.5360	N				0.0606	2.3	3.1	:
		2019.6127	N				0.0318	2.8	5.2	
14206−7516	**	2019.5386	N				0.1920	1.7	2.5	:
		2020.2006	Y	0.0877	154.0	0.0				:
14396−6050	none	2019.5333	N				0.0477	2.5	4.3	
		2020.1118	N				0.0437	2.8	4.4	
14341−1824	**	2020.1172	Y	0.1438	64.6	1.3				
14343−1231	none	2019.5387	N				0.0477	2.6	4.4	
		2020.1174	N				0.0450	2.4	4.1	
14441−3427	none	2020.1172	N				0.0508	2.6	3.5	
14542−2042	**	2020.1172	Y	0.3018	351.4	1.1				q
14545+1606	Mar00	2019.5360	N				0.1312	2.0	2.0	:
15095−1547	**	2020.1174	Y	0.5795	199.0	2.1				p
15157−0725	**	2019.5387	Y	0.5390	26.2	0.1				
		2020.1119	Y	0.5311	28.2	0.0				
15194−0743	none	2019.5387	N				0.0450	2.5	4.4	
15248−4930	none	2019.5363	N				0.0485	2.2	3.7	
		2020.1118	N				0.0534	2.6	4.4	
15309−6801	**	2019.5386	Y	0.3354	304.4	1.2				:
		2020.1119	Y	0.2936	305.1	1.2				q
15319+2851	*	2019.6125	Y	0.0952	13.3	0.0				:
15421−1928	none	2020.1119	N				0.0470	2.4	4.1	
15457−4330	*	2019.5364	Y	0.2538	335.6	2.5				q
		2020.1119	Y	0.2345	335.1	2.5				q
15467−5535	*	2019.5363	Y	0.2715	12.3	1.6				q
		2020.1118	Y	0.2625	29.8	1.6				:
15474−1054	*	2019.5387	Y	0.2282	241.1	0.9				q
		2020.1119	Y	0.1837	226.6	0.8				q
		2020.2008	Y	0.1774	224.3	1.0				q
15476−2754 CD	**	2019.5364	Y	0.1051	150.5	0.2				
		2020.1119	Y	0.0740	163.5	0.0				:
15578−5132	**	2019.5363	Y	0.3261	331.9	0.8				q

Table 2 *continued on next page*

Table 2 *(continued)*

WDS (1)[a]	First res. (2)[b]	Date obs. (year) (3)	Resol. (Y/N) (4)	ρ ($''$) (5)[c]	θ (deg) (6)[c]	Δm (mag) (7)[c]	$\rho_{\min}$ ($''$) (8)[d]	Δm ($0.''15$) (mag) (9)[d]	Δm ($1.''0$) (mag) (10)[d]	Obs. flags (11)[e]
		2020.1119	Y	0.3541	333.6	0.9				q
16019−3357	**	2019.5364	Y	0.6939	61.6	0.2				p
		2020.1119	Y	0.6714	61.3	0.0				p
16170−3137	**	2019.5365	Y	0.2691	46.2	0.2				
		2020.2007	Y	0.2790	37.1	0.0				
16202−3734 A	none	2019.5364	N				0.0534	2.1	3.2	
16269−3813	none	2019.5364	N				0.0643	2.1	3.0	
17129−0508	none	2019.5361	N				0.0492	2.2	3.3	
17137−0825	*	2019.5361	Y	0.0345	30.7	0.2				
		2019.6128	Y	0.0401	54.8	0.2				
		2020.2008	Y	0.0420	148.0	0.0				
17177+1140	none	2019.5361	N				0.0573	2.2	2.9	
17282−0144	**	2019.5361	Y	0.0736	22.7	0.7				
17298−2504	**	2019.5338	Y	0.1435	203.3	0.5				
		2020.2008	Y	0.1659	201.5	0.6				
17365−2515	**	2019.5338	Y	0.4553	258.1	1.4				:
		2020.2008	Y	0.4543	257.3	1.8				:
17371−4419	War15	2019.5365	N				0.0437	2.3	4.2	
		2020.2008	N				0.0415	3.6	5.3	
17462−3206	none	2019.6129	N				0.0636	2.5	4.3	
		2020.2008	N				0.0415	2.6	4.9	
17466−5719	none	2020.2009	N				0.0415	2.2	5.6	
18036−1859	*	2019.5338	Y	0.2190	351.9	1.3				q
		2020.8228	Y	0.1648	325.3	1.4				q
18097−0220	none	2019.5361	N				0.0583	2.1	2.6	
18099−1027	**	2019.5361	Y	0.7285	36.2	0.2				p
		2020.8228	Y	0.7596	37.8	0.3				p
18268−6543	none	2019.5365	N				0.0926	1.9	2.4	
		2020.8337	N				0.2250	1.6	1.6	:
18411+2447	none	2019.6130	N				0.0543	2.4	3.6	
18460−2856	*	2019.6130	Y	0.3485	182.3	1.4				q
		2020.7694	Y	0.3949	172.4	1.4				q
18483−6856	Jao14	2020.8337	N				0.2864	1.8	1.8	:
18555+0824	none	2019.5363	N				0.0457	2.2	3.3	
18597−6327	**	2019.5366	Y	0.0563	44.8	0.3				
		2020.7693	Y	0.0297	20.8	0.0				:
		2020.8364	Y	0.0343	11.4	0.0				
19127−3615	none	2019.6130	N				0.0636	2.4	4.2	
		2020.8364	N				0.0508	2.7	3.7	
19208−4534	none	2019.6129	N				0.0492	2.5	4.5	
19216+2052	none	2019.6130	N				0.0573	2.6	3.4	
19242−0932	**	2019.5339	Y	0.4212	64.2	0.3				:
		2020.8228	Y	0.4321	239.3	0.3				q
19310−7337	**	2019.5366	Y	0.6704	175.4	3.5				q
		2020.7693	Y	0.6299	169.1	3.5				
19341−5225	none	2019.5366	N				0.0534	2.4	3.7	
		2020.2009	N				0.0415	2.4	5.1	
19420−2104	none	2019.5391	N				0.0716	2.4	4.2	
		2020.8364	N				0.0516	2.7	3.9	
19468−0158	none	2019.5339	N				0.0543	2.4	3.9	
		2020.8228	N				0.0500	2.6	4.1	
19517−3100	*	2019.5391	Y	0.1215	13.8	1.9				q
		2019.8564	Y	0.1567	22.3	1.9				q

Table 2 *continued on next page*

Table 2 *(continued)*

WDS (1)[a]	First res. (2)[b]	Date obs. (year) (3)	Resol. (Y/N) (4)	ρ ($''$) (5)[c]	θ (deg) (6)[c]	Δm (mag) (7)[c]	$\rho_{\rm min}$ ($''$) (8)[d]	Δm ($0.''15$) (mag) (9)[d]	Δm ($1.''0$) (mag) (10)[d]	Obs. flags (11)[e]
		2020.8339	Y	0.1274	37.4	1.9				
19544−3148	**	2019.5391	Y	0.1367	139.5	0.8				q
		2019.8564	Y	0.1409	147.4	0.9				q
		2020.8339	Y	0.1555	167.4	0.8				q
20154−5646	**	2019.5366	Y	0.7991	31.2	1.8				p
		2020.8337	Y	0.8113	34.8	1.3				p
20253−2259	**	2019.5391	Y	0.9363	270.6	0.2				:
		2020.8229	Y	0.9338	268.8	0.4				p
20492−4012	*	2019.5392	Y	0.0938	20.2	1.1				
		2019.6135	Y	0.0976	20.9	1.2				q
		2020.8284	N				0.0500	2.4	3.7	
		2020.9241	Y	0.0490	186.6	1.4				
20556−1402	*	2018.4853	Y	0.0811	302.9	0.4				q
		2018.8050	Y	0.0751	239.8	0.4				
		2019.5287	Y	0.1024	235.6	0.3				
		2019.8563	Y	0.1027	197.7	0.4				q
		2020.8339	Y	0.0589	189.6	0.0				
21011−4907	none	2019.5392	N				0.0636	2.6	4.1	
		2020.8337	N				0.0534	2.5	3.5	
21142−7633	**	2019.6132	Y	0.7786	68.9	0.8				p
		2020.8336	Y	0.8351	69.7	0.8				:
21176−4445	**	2019.5392	Y	0.7954	357.8	0.0				
		2020.7694	Y	0.7725	357.5	0.1				:
21202−6739	none	2019.6132	N				0.0492	2.6	4.0	
		2020.8337	N				0.0508	3.0	4.3	
21283−2219	none	2019.9495	N				0.0415	2.2	4.7	
		2020.8339	N				0.0508	2.7	4.2	
21296+1739	*	2019.5394	N				0.0525	2.8	4.3	
		2019.8563	Y	0.0367	96.4	0.0				
		2020.8228	Y	0.0307	209.0	0.2				
		2020.8228	Y	0.0250	193.9	0.0				*y*
21308−4043	none	2019.5392	N				0.0636	2.7	4.2	
		2019.8564	N				0.0477	2.4	4.0	
		2020.8339	N				0.0508	2.6	3.9	
21344−4316	none	2019.8564	N				0.0643	2.2	3.3	
21364−4401	none	2020.8339	N				0.0534	2.5	3.3	
21387−3340	none	2019.5392	N				0.0636	2.6	4.4	
		2019.8564	N				0.0470	2.8	4.2	
		2020.8339	N				0.0508	2.7	4.1	
21390−2409	none	2019.5392	N				0.0741	2.1	3.5	
		2020.8339	N				0.0516	2.8	3.7	
21497−4139	*	2019.5392	Y	0.2030	320.5	1.6				q
		2019.8564	Y	0.1934	317.1	1.6				q
		2020.7694	Y	0.1540	303.6	1.5				:
		2020.9242	Y	0.1495	302.6	1.7				q
21558−3313	**	2019.5392	N				0.0708	2.4	4.0	
		2019.8564	Y	0.0490	207.8	1.1				
		2020.8339	Y	0.0420	229.1	0.8				
21569−0154	none	2020.8339	N				0.0716	2.0	2.7	
21588−3226	none	2019.5392	N				0.1260	1.2	1.8	:
		2019.8566	N				0.0643	2.3	3.1	
22025−3705	none	2019.5392	N				0.0636	2.8	4.6	
		2019.8566	N				0.0444	2.6	4.2	

Table 2 *continued on next page*

Table 2 *(continued)*

WDS (1)[a]	First res. (2)[b]	Date obs. (year) (3)	Resol. (Y/N) (4)	ρ ($''$) (5)[c]	θ (deg) (6)[c]	Δm (mag) (7)[c]	$\rho_{\rm min}$ ($''$) (8)[d]	Δm ($0\farcs15$) (mag) (9)[d]	Δm ($1\farcs0$) (mag) (10)[d]	Obs. flags (11)[e]
22067−4458	*	2019.5392	Y	0.2757	147.3	2.7				:
		2020.8339	Y	0.2990	144.5	2.7				:
22167−4801	**	2019.5367	Y	0.2036	240.3	2.7				q
		2019.8566	Y	0.1962	236.7	2.6				q
		2020.7694	Y	0.1576	224.8	2.6				:
22173−3444	**	2019.5392	Y	0.0734	76.4	0.0				:
		2019.6134	Y	0.0726	73.1	0.0				
		2019.8566	Y	0.0856	55.5	0.2				
		2019.9495	Y	0.0900	49.0	0.1				
		2020.8341	Y	0.1636	28.4	0.0				
22231−1736	none	2019.5393	N				0.0685	2.3	3.9	
22302−5345	*	2019.5367	Y	0.1620	80.1	1.1				q
		2019.6135	Y	0.1530	79.5	1.1				q
		2019.8566	Y	0.1457	76.2	1.1				q
		2019.9495	Y	0.1424	74.3	1.2				q
		2020.8337	Y	0.0668	41.9	0.9				:
22351−4218	Kar20	2019.5393	Y	0.4275	350.7	0.0				
		2019.8566	Y	0.4234	351.7	0.0				
		2020.8341	Y	0.4009	354.8	0.0				
22388−2037 BD	none	2019.5393	N				0.0525	2.6	4.2	
22388−2037 AC	none	2019.5393	N				0.0450	2.6	4.9	
		2019.8566	N				0.0404	2.7	4.0	
22486−3109	none	2019.5393	N				0.0636	2.6	4.2	
		2019.8566	N				0.0470	3.0	4.2	
23059−3551	War15	2019.5393	N				0.0409	2.7	4.9	
		2020.8341	N				0.0399	2.8	4.3	
23073−0416	**	2019.5396	Y	0.4514	111.6	2.1				q
		2019.8563	Y	0.4533	109.5	2.1				q
		2020.8340	Y	0.4470	103.8	2.0				q
23083−1525	**	2019.5396	N				0.0500	2.8	4.3	
		2019.8566	N				0.0437	2.9	4.2	
		2020.9241	Y	0.0307	102.9	1.0				:
23107−1914	none	2020.8342	N				0.0508	2.7	4.0	
		2020.9242	N				0.0415	3.2	5.0	
23120−1702	**	2019.5396	Y	0.4874	34.0	0.0				:
		2019.8566	Y	0.4960	35.1	0.0				
		2020.8342	Y	0.5199	38.1	0.0				
23242−1746	**	2019.9495	Y	0.0689	359.3	0.0				
		2020.8342	Y	0.1177	19.3	0.0				
		2020.9242	Y	0.1195	20.4	0.1				q
23254−6740	**	2019.6132	Y	0.1376	78.3	0.0				
		2019.8567	Y	0.1274	84.6	0.0				
		2019.9495	Y	0.1269	86.6	0.0				
		2020.7694	Y	0.1118	103.0	0.0				:
23302−2023	none	2018.9746	N				0.0415	2.7	5.3	
		2020.9242	N				0.0415	2.8	5.4	
23369−3629	none	2019.5367	N				0.0508	2.5	3.4	
		2020.8341	N				0.0525	2.6	3.7	
23486−2740	none	2019.5367	N				0.0477	2.4	3.6	
		2020.8342	N				0.0534	2.7	3.7	
23524−1441	**	2019.5367	Y	0.3780	252.9	1.9				q
		2019.9495	Y	0.3781	250.3	1.9				q
		2020.8342	Y	0.3801	245.4	1.8				:

Table 2 *continued on next page*

Table 2 *(continued)*

WDS	First res.	Date obs. (year)	Resol. (Y/N)	ρ ($''$)	θ (deg)	Δm (mag)	$\rho_{\rm min}$ ($''$)	Δm ($0.''15$) (mag)	Δm ($1.''0$) (mag)	Obs. flags
(1)[a]	(2)[b]	(3)	(4)	(5)[c]	(6)[c]	(7)[c]	(8)[d]	(9)[d]	(10)[d]	(11)[e]
23548−0957	**	2019.5396	Y	0.2525	249.5	2.6				q
		2019.8590	Y	0.2636	251.1	2.5				q
		2020.8342	Y	0.2842	262.4	2.6				q
23557−0609	**	2019.5396	Y	0.3082	59.3	4.3				
		2019.8590	Y	0.2890	53.0	4.6				
		2020.8342	Y	0.2434	40.1	4.2				
23585+0740	**	2018.5617	Y	0.1808	171.8	2.4				
		2019.5397	Y	0.2501	176.5	2.3				q
		2020.8340	Y	0.2211	181.8	2.6				q

References— Jan14 = Janson et al. (2014), Jao14 = Jao et al. (2014), Jod13 = Jódar et al. (2013), Kar20 = Karmakar et al. (2020), Mar00 = Martín et al. (2000), War15 = Ward-Duong et al. (2015)

[a] Column 1 — For resolved systems not already noted in the WDS catalog (Mason et al. 2001), the WDS code given is the anticipated code for the future entry.

[b] Column 2 — This column gives a single or double asterisk (* or **) for each new resolution, depending on previous status of the target's multiplicity. A single asterisk (*) indicates a new resolution of a system already known in the literature to be a multiple, but which has never previously been resolved. A double asterisk (**) marks a new resolution of a system that was previously a multiple candidate at best, with its multiplicity not established in the literature; these are new multiples. Systems previously resolved by others have their first resolution reference listed. Systems not resolved here and never resolved previously are noted with "none" in this column.

[c] Columns 5–7 — For observations that resolved a companion, these columns give the separation (ρ), position angle (θ), and magnitude difference (Δm) between components.

[d] Columns 8–10 — For observations with no detected companion, these columns provide limits: the minimum separation distinguishable ($\rho_{\rm min}$) for pairs with $\Delta m < 1$ mag, the magnitude difference limit at $0.''15$ from the primary source, and the magnitude difference limit at $1.''0$ from the source.

[e] Column 11 — This column contains flags related to each observation: q = quadrant has been determined, p = Δm determined photometrically from average image, : = noisy data, y = magnitude difference in y band (all others in I band).

Table 3. Summary of SOAR speckle results for each of the three sample subsets, as well as the targets meeting the formal multiplicity criteria in DR2 (Vrijmoet et al. 2020) and the full sample.

Subset name	Targets observed	Pairs resolved	Percent resolved	Targets not observed
(1)	(2)	(3)	(4)	(5)
0.9 m PB	120	59	49%	3
Literature multiples	188	140	74%	1
DR2 suspects	249	188	76%	3
2+ DR2 criteria	217	176	81%	2
Full sample[a]	333	211	63%	5

[a] Numbers are not the sums of the four categories above because of overlaps in samples, as shown in the Venn diagram of Figure 1.

Table 4. Elements of the best-fit relative orbits shown in Figure 3. These orbits have been fit to the relative positions of the systems' components using all resolutions (including literature and this SOAR program), as well as radial velocities if those data are available.

Name	WDS	Discov code	P (yr)	a (mas)	e	i (deg)	Ω (deg)	ω (deg)	T_0 (yr)	Additional data used
(1)	(2)	(3)	(6)	(7)	(8)	(9)	(10)	(11)	(12)	(13)
G 131-026 AB	00089+2050	BEU 1	5.918 ± 0.017	144.0 ± 4.6	0.106 ± 0.023	145.67 ± 3.29	83.61 ± 6.59	240.38 ± 17.17	2018.921 ± 0.173	Beu04, Jan14, Hor15
2MA 0015-1636 AB	00160−1637	BWL 2	4.187 ± 0.039	108.0 ± 7.2	0.433 ± 0.090	63.63 ± 2.11	111.81 ± 5.15	98.03 ± 4.82	2021.145 ± 0.057	Bow15
LP 993-115 BC	02452−4344	BRG 15Aa,Ab	28.466 ± 2.056	630.3 ± 37.5	0.240 ± 0.029	117.13 ± 1.98	158.70 ± 1.01	305.03 ± 8.74	2009.714 ± 0.434	Ber10, Jan12, Jan14
SCR 0533-4257 AB	05335−4257	SYU 7	0.672 ± 0.003	54.4 ± 3.3	0.490 ± 0.066	150.73 ± 9.59	109.41 ± 29.17	44.38 ± 9.59	2017.155 ± 0.013	Sha17
LHS 501 AC	20556−1402	... ...	1.855 ± 0.014	91.6 ± 1.2	0.242 ± 0.008	142.67 ± 2.11	236.06 ± 2.46	232.05 ± 1.88	2017.135 ± 0.009	Bar18[a]

References— Bar18 = Baroch et al. (2018), Ber10 = Bergfors et al. (2010), Beu04 = Beuzit et al. (2004), Bow15 = Bowler et al. (2015), Hor15 = Horch et al. (2015), Jan12 = Janson et al. (2012), Jan14 = Janson et al. (2014), Sha17 = Shan et al. (2017)

[a] RV data used in orbit fit.